REPORT DOCUMENTATION PAGE

The public reporting burden for this collection of information is estimated to average 1 hour per response, including the time for reviewing instructions, searching existing data sources, gathering and maintaining the data needed, and completing and reviewing the collection of information. Send comments regarding this burden estimate or any other aspect of this collection of information, including suggestions for reducing the burden, to the Department of Defense, Executive Services and Communications Directorate (0704-0188). Respondents should be aware that notwithstanding any other provision of law, no person shall be subject to any penalty for failing to comply with a collection of information if it does not display a currently valid OMB control number.
PLEASE DO NOT RETURN YOUR FORM TO THE ABOVE ORGANIZATION.

1. REPORT DATE *(DD-MM-YYYY)*	2. REPORT TYPE	3. DATES COVERED *(From - To)*
18-06-2014	Journal Article	

4. TITLE AND SUBTITLE	5a. CONTRACT NUMBER
Observations on stratified flow over a bank at low Froude numbers	
	5b. GRANT NUMBER
	5c. PROGRAM ELEMENT NUMBER
	0602435N

6. AUTHOR(S)	5d. PROJECT NUMBER
Ewa Jarosz, Hemantha W. Wijesekera, William J. Teague, Diane B. Fribance, and Mark A. Moline	
	5e. TASK NUMBER
	5f. WORK UNIT NUMBER
	73-4491-04-5

7. PERFORMING ORGANIZATION NAME(S) AND ADDRESS(ES)	8. PERFORMING ORGANIZATION REPORT NUMBER
Naval Research Laboratory Oceanography Division Stennis Space Center, MS 39529-5004	NRL/JA/7330--13-2019

9. SPONSORING/MONITORING AGENCY NAME(S) AND ADDRESS(ES)	10. SPONSOR/MONITOR'S ACRONYM(S)
Office of Naval Research One Liberty Center 875 North Randolph Street, Suite 1425 Arlington, VA 22203-1995	ONR
	11. SPONSOR/MONITOR'S REPORT NUMBER(S)

12. DISTRIBUTION/AVAILABILITY STATEMENT

Approved for public release, distribution is unlimited.

13. SUPPLEMENTARY NOTES

14. ABSTRACT

In June 2011, a 9 day oceanographic survey was conducted over the East Flower Garden Bank, a coral reef, located on the outer shelf in the northwestern Gulf of Mexico. Current, temperature, conductivity, and microstructure measurements were collected to characterize flow evolution, turbulence, and mixing over the bank. During the experiment, the flow was highly stratified, subcritical (Froude number below 0.4), hydrostatic, and nonlinear with rotational effects being important. Observations showed that flow structure, turbulence, and mixing were highly dependent on the direction and strength of the current; thus, they varied spatially and temporally. Responses resulting from interactions between the free-stream flow and the obstacle were significantly different on the upstream and downstream sides of the bank. Blocking and diverging of the flow just below the bank height was observed on the upstream side. On the downstream side, a wake with imbedded vortices developed. Moreover, turbulence was amplified over the bank top and on its downstream side. Turbulent dissipation rates were as high as 1026 W kg21 and resulted in measured rates of energy dissipation and mixing by turbulence per unit width as high as 40 W m21. Mixing in the downstream side was elevated with eddy diffusivities reaching 1023 m2 s21, well above a typical value of 1025 m2 s21 commonly found in the ocean thermocline and over shelves with flat topography. On the upstream side, estimated eddy diffusivities were close to that for the ocean thermocline, i.e., they were generally less than 0.531024 m2 s21.

15. SUBJECT TERMS

subcritical flow; underwater bank; mixing; Gulf of Mexico

16. SECURITY CLASSIFICATION OF:			17. LIMITATION OF ABSTRACT	18. NUMBER OF PAGES	19a. NAME OF RESPONSIBLE PERSON
a. REPORT	b. ABSTRACT	c. THIS PAGE			Ewa Jarosz
Unclassified	Unclassified	Unclassified	UU	19	19b. TELEPHONE NUMBER *(Include area code)* (228) 688-4292

Reset

UBLICATION OR PRESENTATION RELEASE REQUEST

13-1231-4038

NRLINST 5600.2

Ref: (a) NRL Instruction 5600.2
(b) NRL Instruction 5510.40D

Encl: (1) Two copies of subject paper
(or abstract)

( ) Abstract only, published
( ) Book
( ) Conference Proceedings (refereed)
( ) Invited speaker
(X) Journal article (refereed)
( ) Oral Presentation, published
( ) Other, explain

( ) Abstract only, not published
( ) Book chapter
( ) Conference Proceedings (not refereed)
( ) Multimedia report
( ) Journal article (not refereed)
( ) Oral Presentation, not published

STRN NRL/JA/7330-13-2019
Route Sheet No. 7330/
Job Order No. 73-4491-04-5
Classification X U
Sponsor ONR BASE 6.1
approval obtained ..... yes X no

Title of Paper or Presentation
Observations on Stratified Flow Over a Bank at Low fFroude Numbers

Author(s) Name(s) (First, MI, Last), Code, Affiliation if not NRL

Ewa Jarosz 7332 Hemantha W Wijesekera 7332 William J. Teague 7332 Diane Fribance Coastal Carolina Univ. - SC Mark Moline CA Polytechnic Univ.

It is intended to offer this paper to the _____
                                                                 (Name of Conference)

_____
(Date, Place and Classification of Conference)

and/or for publication in **Journal of Geophysical Research, Unclassified**
                              (Name and Classification of Publication)   (Name of Publisher)

After presentation or publication, pertinent publication/presentation data will be entered in the publications data base, in accordance with reference (a).
It is the opinion of the author that the subject paper (is ____) (is not ___ X) classified, in accordance with reference (b).
This paper does not violate any disclosure of trade secrets or suggestions of outside individuals or concerns which have been communicated to the Laboratory in confidence. This paper (does ____) (does not ___ X) contain any militarily critical technology.
This subject paper (has ____) (has never __ X) been incorporated in an official NRL Report.

Ewa Jarosz, 7332
Name and Code (Principal Author)   (Signature)

CODE	SIGNATURE	DATE	COMMENTS
Author(s) Jarosz	Will J Teague	12/17/13	Need by ____ 08 Jan 14
			Publicly accessible sources used for this publication
			This is a Final Security Review. Any changes made in the document, after approved by Code 1231, nullify the Security Review.
Section Head Teague	Will J Teague	12/17/13	
Branch Head Richard L. Crout, 7330		12-17-2013	1. Release of this paper is approved. 2. To the best knowledge of this Division, the subject matter of this paper (has ____) (has never __ X) been classified.
Division Head Ruth H. Preller, 7300		12/17/13	
Security, Code 1231		12/17/13	1. Paper or abstract was released. 2. A copy is filed in this office.
Office of Counsel, Code 1008.3	Randy Chapman	12/19/13	
ADOR/Director NCST E. R. Franchi, 7000			
Public Affairs (Unclassified/ Unlimited Only), Code 7030.4	Shannon Mensi	12-19-13	17 DEC '13 PM 1:17
Division, Code			
Author, Code			

THIS FORM CANCELS AND SUPERSEDES ALL PREVIOUS VERSIONS

JGR

RESEARCH ARTICLE

Key Points:
- Observations showed complex flow over the East Flower Garden Bank in June 2011
- Flow was blocked and diverged upstream of the bank
- A wake with elevated turbulence and mixing developed downstream of the bank

Correspondence to:
E. Jarosz,
ewa.jarosz@nrlssc.navy.mil

Observations on stratified flow over a bank at low Froude numbers

Ewa Jarosz[1], Hemantha W. Wijesekera[1], William J. Teague[1], Diane B. Fribance[2], and Mark A. Moline[3]

[1]Naval Research Laboratory, Stennis Space Center, USA, [2]Department of Marine Science, Coastal Carolina University, Conway, South Carolina, USA, [3]School of Marine Science and Policy, University of Delaware, Lewes, Delaware, USA

Abstract In June 2011, a 9 day oceanographic survey was conducted over the East Flower Garden Bank, a coral reef, located on the outer shelf in the northwestern Gulf of Mexico. Current, temperature, conductivity, and microstructure measurements were collected to characterize flow evolution, turbulence, and mixing over the bank. During the experiment, the flow was highly stratified, subcritical (Froude number below 0.4), hydrostatic, and nonlinear with rotational effects being important. Observations showed that flow structure, turbulence, and mixing were highly dependent on the direction and strength of the current; thus, they varied spatially and temporally. Responses resulting from interactions between the free-stream flow and the obstacle were significantly different on the upstream and downstream sides of the bank. Blocking and diverging of the flow just below the bank height was observed on the upstream side. On the downstream side, a wake with imbedded vortices developed. Moreover, turbulence was amplified over the bank top and on its downstream side. Turbulent dissipation rates were as high as 10^{-6} W kg^{-1} and resulted in measured rates of energy dissipation and mixing by turbulence per unit width as high as 40 W m^{-1}. Mixing on the downstream side was elevated with eddy diffusivities reaching 10^{-3} m^2 s^{-1}, well above a typical value of 10^{-5} m^2 s^{-1} commonly found in the ocean thermocline and over shelves with flat topography. On the upstream side, estimated eddy diffusivities were close to that for the ocean thermocline, i.e., they were generally less than 0.5×10^{-4} m^2 s^{-1}.

1. Introduction

Substantial research efforts in past decades have been devoted to studying flows over rough bottom topography in the ocean. They have led to the conclusion that mixing is much greater there than mixing over a gradually varying seabed or in the thermocline in the open ocean [e.g., *Gregg*, 1987; *Dewey and Crawford*, 1988; *Ledwell et al.*, 1993; *Lueck and Mudge*, 1997]. Significant bathymetric features such as sills, canyons, banks, seamounts, ridges, underwater volcanos, and mountain ranges are ubiquitous in the ocean. They impact flow patterns locally, and they may even influence large-scale circulation [e.g., *Kunze and Toole*, 1997; *Polzin et al.*, 1997; *Nash and Moum*, 2001; *Rudnick et al.*, 2003; *McCabe et al.*, 2006].

On continental shelves, small banks are fairly common features. Their spatial dimensions can vary greatly from a few hundred meters to several kilometers; however, they are often too small to be included in numerical models developed for the coastal waters. As a result, flow, stratification, mixing, and biochemical processes are not well resolved by numerical simulations near such bathymetric structures. In situ observations have shown [e.g., *Loder et al.*, 1992; *Moum and Nash*, 2000; *Nash and Moum*, 2001; *Dewey et al.*, 2005] that underwater banks significantly alter ambient flow, considerably increase density gradients, modify vertical current shear, and enhance turbulence. Stratified flow approaching an obstacle often accelerates, and to conserve momentum, mechanical energy is released that can be dissipated locally or radiated away through internal waves. As a result, lee waves, hydraulic jumps, and eddies are very common features near banks. Amplified turbulence over a bank usually accounts for a large fraction of the entire shelf mixing, exerts a larger bottom stress, and dissipates a significant amount of energy in a shelf region [e.g., *Moum and Nash*, 2000].

Stratified flows over an obstacle are often categorized as subcritical, critical, and supercritical in terms of the Froude number that is defined as a ratio of the flow speed to the buoyancy frequency and the total depth. Evolution of flows and their major features vary dramatically as a function of the Froude
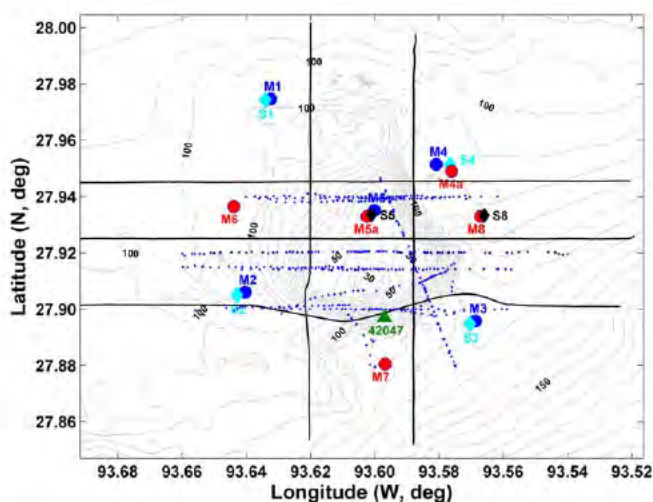
JAROSZ ET AL.   6403

Figure 1. Map of the East Flower Garden Bank with depth contours (gray lines) every 5 m; also shown are locations of the long term Barny (M1 M4; blue circles) and string (S1 S4; cyan diamonds) moorings, short term Barny (M4a, M5a, M6 M8; red circles) and string (S5 and S8; black diamonds) moorings, VMP drops (blue dots), selected ScanFish tows (black lines), and meteorological buoy 42047.

number. Past observational and modeling efforts in the ocean have often been focused on studying energetic flows with Froude numbers approaching 1 or larger, i.e., critical and supercritical flows over rough topography with energy being released through, for instance, a hydraulic jump [e.g., *Wesson and Gregg*, 1994; *Farmer and Armi*, 1999; *Hogg et al.*, 2001; *Moum and Nash*, 2000]. Much of our understanding of flow dynamics for very low Froude numbers (much less than 1) comes mostly from the atmospheric research of subcritical airflows over a mountain [e.g., *Hunt and Snyder*,

1980; *Smolarkiewicz and Rotunno*, 1989; *Smith and Grønås*, 1993; *Vosper et al.*, 1999; *Dalziel et al.*, 2011]. These airflows are usually characterized by blocking, splitting, and moving around on the upstream side of the obstacle. On its downstream side, a wake develops where enhanced turbulence and eddy shedding are commonly observed.

In this paper, recent current and hydrographic observations are analyzed to describe the evolution and main features of the subcritical highly stratified flow over an isolated bank located on the outer northwestern Louisiana-Texas shelf in the Gulf of Mexico. Moreover, collected microstructure measurements allow an assessment of turbulence and mixing in this region. The paper is organized as follows. In section 2, the bank, field experiment, and observations are described. Background meteorological and oceanographic conditions are discussed in section 3. Snapshots of flow patterns and stratification are presented in section 4. Turbulence and mixing conditions over the bank are characterized in section 5. In section 6, a discussion of the results in terms of nondimensional parameters is presented. Finally, findings are summarized in section 7.

2. East Flower Garden Bank Experiment

The field experiment was a part of the MORT ("Mixing over Rough Topography") and COB ("Currents over Bank") projects funded by the Naval Research Laboratory (NRL) and the Bureau of Ocean Energy Management (BOEM), respectively. It took place from 31 May 2011 to 13 June 2011 over and around the East Flower Garden Bank (EFGB). The EFGB is located on the shelf edge in the northwestern Gulf of Mexico about 190 km southeast of Galveston, TX (Figure 1). The bank is a thriving coral reef. It is a part of the Flower Garden Banks National Marine Sanctuary managed by NOAA, and is one of many banks formed by salt domes on the Louisiana-Texas shelf. The EFGB is asymmetric with rather steep slopes on its southern and eastern sides. It is about 10 km long and 6 km wide with major and minor axes approximately aligned in north-south and east-west directions, respectively. The bank top rises from water depths of 100–130 m to about 18 m below the sea surface. The ocean bottom area covered by the bank (within a 100 m isobath) is about 40.76 km^2.

Two research vessels, R/V Pelican and R/V Manta, occupied waters over the bank to measure currents, hydrography, and turbulent mixing. Almost all data collected by instruments deployed from or towed by the ships were taken between 4 June 2011 and 12 June 2011. Both vessels were equipped with 300 kHz acoustic Doppler current profilers (ADCPs) to collect current velocity profiles with vertical resolution of 4 m. Velocity observations were processed using the University of Hawaii's CODAS system [*Firing et al.*, 1995] to correct for ship motion and averaged over 4 min intervals. A towed undulating vehicle, ScanFish MK II,

manufactured by EIVA of Denmark and equipped with a Sea-Bird Electronics SBE 49 FastCAT was used to sample hydrography from the R/V Pelican. Conductivity, temperature, and microstructure observations were collected with a Vertical Microstructure Profiler (VMP; the profiler was manufactured by the Rockland Oceanographic Services Inc., Canada and is similar to a profiler described by *Wolk et al.* [2002]) from the R/V Manta. The VMP profiler carried a thermistor (FP07), a microconductivity sensor (Sea-Bird Electronics SBE7-38), two velocity shear probes, a high-resolution pressure sensor, accelerometers, and fine-scale external conductivity (Sea-Bird Electronics SBE4) and temperature (Sea-Bird Electronics SBE3) sensors. VMP profiles extended from a few meters below the surface to near the bottom. Moreover, turbulent kinetic energy (TKE) dissipation rates (ε) were estimated from small-scale velocity shear following a formula for isotropic turbulence [*Oakey*, 1982]: $\varepsilon \approx \frac{15}{2}\nu\overline{\left(\frac{\partial u'}{\partial z}\right)^2}$, where ν is the kinematic viscosity, and $\overline{\left(\frac{\partial u'}{\partial z}\right)^2}$ is the variance of the current shear. The velocity shear variance was calculated by integrating the spectrum for the wave number range from 2 to 30 cpm (cycles per meter), while the spectrum was estimated in bins of 1024 shear-probe data records, with a 512-record overlap. Selected ScanFish sections and locations of VMP drops are displayed in Figure 1.

Additionally, two dye releases were conducted from the R/V Pelican to visualize flow patterns over and around the EFGB. The first release was on the western side of the bank around 21:00 UTC on 6 June 2011. The dye was released near the top of the thermocline ($\sim$30 m). The second dye patch was also released near the depth of $\sim$ 30 m but on the eastern side of the bank at about 15:00 UTC on 8 June 2011. The dye used in the experiment was a water soluble fluorescein dye (Keyacid Uranine K Liquid) referred as "Uranine" (www.dyes.com). The density of the liquid Uranine (40% concentrate) was 1111 kg m^{-3}. The dye concentration was reduced to 12% to obtain a target density close to 1023.79 ($\pm$0.01) kg m^{-3} by adding 662.4 L of freshwater and 45.4 L of isopropyl alcohol. The dye was released to the sea through a diffuser (of about 1 m length) attached to the end of a hose. The dye volume of $\sim$1022.1 L was pumped at 37.9 L min^{-1} while the R/V Pelican streamed at a speed of about 1 m s^{-1} in the north-south direction. The depressor undulated approximately $\pm$2 m from the 30 m depth. We planned for a dye patch of 1 m wide, 2 m high, and 1.1 km long with the initial dye concentration of 14 mg L^{-1} (or 14 ppm). The dye was sampled by fluorometers attached to the ScanFish and a REMUS Autonomous Underwater Vehicle (AUV) [e.g., *Moline et al.*, 2005], and by a WETLabs ac-9 absorption and attenuation meter (a 490 nm absorption channel) installed on the Scan-Fish. Immediately after dye release, the Scanfish was deployed in a lawn mower pattern while undulating between 10 and 40 m water depths to capture the dye distribution. Several hours later, the REMUS AUV was deployed for a duration of 10 h. The ScanFish fluorometer was calibrated to measure a maximum concentration up to 400 ppb with 0.05 ppb resolution so that it was initially out of scale since the dye concentration was greater than 400 ppb; hence, we used the observed linear correlation between the uranine and chlorophyll to recapture the high values of the missing dye concentration.

Ten Barny (trawl-resistant pods) and six string moorings were in place around and on the EFGB during the field experiment (Figure 1). Five Barny (M1–M5) and four string (S1–S4) moorings were already deployed for the COB project and remained in the water for approximately 1 year [*Teague et al.*, 2013]. Another five Barny (M4a, M5a, M6, M7, and M8) and two string (S5 and S8) moorings were deployed just for 2 weeks specifically for the experiment as a part of the MORT project. All Barny moorings contained Teledyne RD ADCPs and either wave-tide gauges (Sea-Bird Electronics SBE26) or high-resolution pressure sensors called Ppods [*Moum and Nash*, 2008]. String moorings were equipped only with temperature/conductivity/pressure (TCP) sensors, except for S8 which also had a downward-looking ADCP. The number of TCP sensors on the string moorings varied between 5 and 12, and they were either Sea-Bird Electronics MicroCAT (SBE37) or In Situ Aqua Troll instruments. Detailed information such as deployment times and depths, sampling rates, ADCP frequency, and bin depth resolutions for all moorings deployed for the COB program is in *Teague et al.* [2013]. Similar details for the MORT moorings are given here in Table 1. ADCPs for the MORT project were 300 kHz Teledyne RDI units, except for moorings M5a and S8, which were furnished with 600 kHz Teledyne RDI current profilers.

3. Atmospheric and Oceanographic Settings

3.1. Atmospheric Conditions
Atmospheric pressure and winds from nearby NDBC buoy 42047 are shown in Figure 2. Atmospheric pressure (Figure 2a) began increasing on 31 May 2011 and remained high with a maximum of 1022.5 hPa

Table 1. Mooring Summary

Mooring	Latitude (N)	Longitude (W)	Water Depth (m)	Start Date End Date	Sampling Rate (s)/ Bin Size (m)[a]	Depth Range or Instrument Depth (m)[b]
Barny Moorings						
M4a	27°56.942′	93°34.563′	106	2 Jun 2011 13 Jun 2011	60/2	10 102
M5a	27°55.983′	93°36.146′	46	1 Jun 2011 12 Jun 2011	60/1	3.7 44.7
M6	27°56.187′	93°38.633′	101	31 May 2011 12 Jun 2011	60/4	12 96
M7	27°52.830′	93°35.806′	120	31 May 2011 12 Jun 2011	120/4	8 112
M8	27°55.983′	93°34.025′	112	31 May 2011 13 Jun 2011	120/4	8 104
TCP Moorings						
S5						
MC1[c]	27°56.013′	93°36.059′	47	3 Jun 2011	30	5.6
MC2				11 Jun 2011	30	17.3
MC3					30	26.0
MC4					30	36.3
MC5					30	45.9
S8						
MC1	27°55.998′	93°33.953′	112	3 Jun 2011	30	6.4
MC2				11 Jun 2011	30	16.7
MC3					30	38.5
MC4					30	49.7
MC5					30	60.7
MC6					30	71.7
MC7					30	78.7
MC8					30	87.7
MC9					30	96.7
MC10					30	110.0
ADCP[d]					60/1	75.7 111.7 73.6[e]

[a]Sampling Rate (s) sampling rates for all sensors used for the MORT project; Bin Size (m) vertical resolution for ADCP instruments only.
[b]Depth Range depth ranges over which ADCP data were collected at Barny moorings and the downward looking ADCP on S8; Instrument Depth depths for MicroCATS.
[c]MC Sea Bird MicroCAT SBE37 instruments.
[d]ADCP the downward looking RDI 600 kHz ADCP on S8.
[e]A depth of the downward looking ADCP on S8.

during the first part of the experiment. After 5 July 2011, it dropped below 1016 hPa. A few days before the experiment began, the winds were fairly strong reaching 10 m s^{-1} (Figure 2b) and blew from the southern quadrant, i.e., from southeast, south, and/or southwest directions. Winds from the southern quadrant are typical for summer months in the northwestern Gulf of Mexico [*Gutierrez de Velasco and Winant*, 1996]. During the sampling time period, winds weakened and dropped below 6 m s^{-1}. Wind directions were variable directions until 8 July 2011. Then they switched again to a summer pattern, i.e., to southeasterlies.

3.2. Oceanographic Conditions

Mean flow (frequency less than 0.6 cycles per day (cpd)) had two phases during the experiment (Figure 3). Figure 3 shows 40 h low-pass current data. Until mid-day on 8 June 2011, mean currents were moderate (40 cm s^{-1} or less) and generally directed eastward. Afterward, the mean currents weakened (30 cm s^{-1} or less) and reversed, flowing toward the west. Note that mean flow was less impacted by the bank at the M1 mooring than at the M4 mooring. M4 was deployed closer to the EFGB and the currents just below the bank height were very weak, especially evident for the eastward flow phase (Figure 3). Higher frequency fluctuations including tides, inertial, and superinertial oscillations are usually superimposed on the mean flow. Barotropic tidal currents are rather weak in the northwestern Gulf of Mexico [*DiMarco and Reid*, 1998]. *Teague et al.* [2013] estimated amplitudes of major tidal constituents M_2, K_1, and O_1 to be between 3 and 5 cm s^{-1} in the EFGB region. Near-inertial oscillations have a period of 25.58 h (close to the O_1 period), and they are generally more energetic than barotropic tides in the northwestern Gulf of Mexico [*Chen et al.*, 1996]. Near the EFGB, the inertial currents were about 15 cm s^{-1} or larger [*Teague et al.*, 2014]. During the
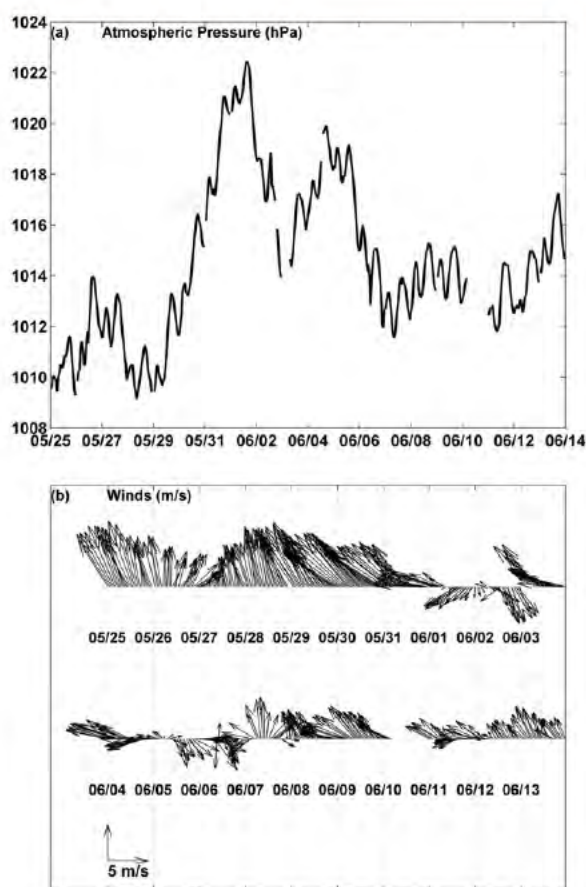
Figure 2. (a) Atmospheric pressure (hPa) and (b) winds (m s^{-1}) a few days before and during the field experiment.

experiment, total measured currents comprised the mean flow, tides, near-inertial currents, and higher frequency motions (frequency higher than 2.4 cpd) and are displayed in Figure 4. Tidal currents showed a spring-neap cycle, while the inertial currents were likely produced by rotating winds at the beginning of June. In the upper 40 m, the currents were as high as 50 and 25 cm s^{-1}, while 40 m depth/time averages were about 20 and 10 cm s^{-1} with standard errors of 1 and 0.5 cm s^{-1} for the eastward and westward mean flows, respectively. All velocity estimates were computed from current observations collected at M1, which seem to be the least impacted by a presence of the EFGB. Only 3.3% of the EFGB area, located just in its southern part, rises above 40 m of the water depth so that the flow above 40 m should have been influenced the least by the bank. This assumption should be especially valid at the M1 mooring located approximately 7 km north of the highest part of the bank. Therefore, 40 m depth current velocity means calculated from M1 observations should be rather good estimates of the free-stream flow velocity and were used in further analyses and discussions.

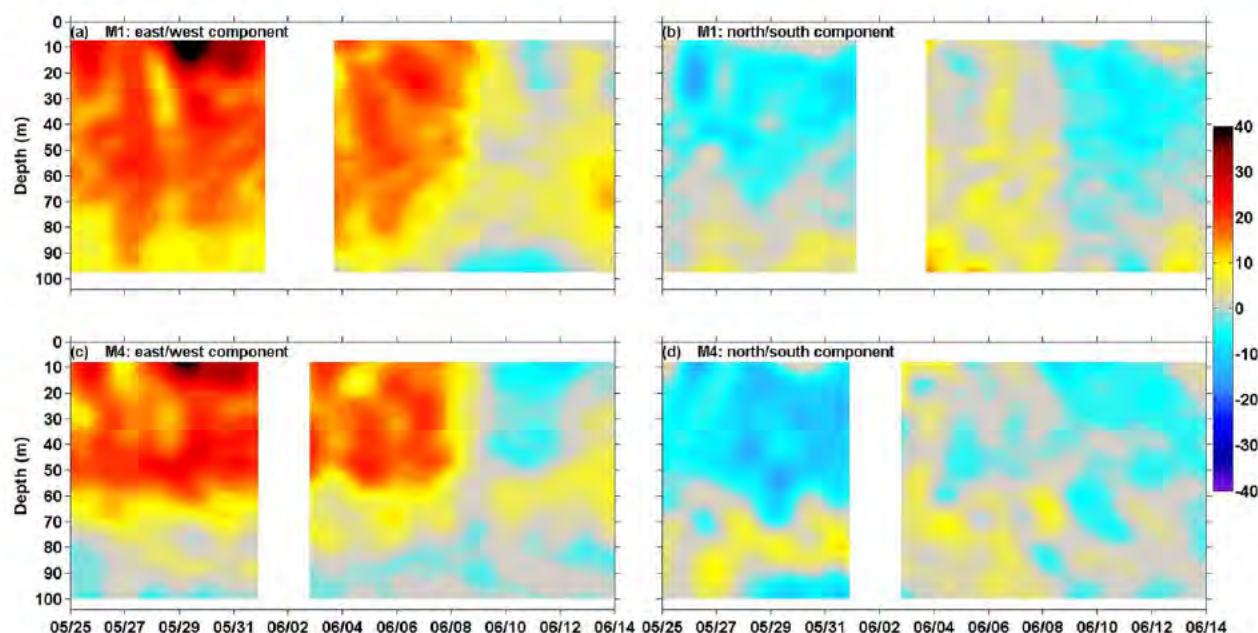Time series of temperature, salinity, and density from S8 are plotted in Figure 5. These observations encompassed almost the entire time period of the field experiment and showed that there was a very shallow mixed layer during this time as also indicated by *Teague et al.* [2013]. Salinity at S8 varied little vertically with a range between 35.20 and 36.66 psu, while temperature showed more variability ranging from 18.10°C near the bottom to 28.64°C at about 6 m below the sea surface. Similar variability and ranges were found at the other TCP moorings. Such distributions of temperature and salinity around the bank generated a mean density that nearly linearly increased with depth as indicated in Figure 6a. Displayed mean densities were calculated from available TCP temperatures and salinities that were averaged over time separately for each mean flow phase, i.e., between 00:00 UTC 4 June and 12:00 UTC 8 June 2011 for the mean eastward flow and between 12:00 UTC 8 June and 23:00 UTC 12 June 2011 for the mean westward flow. The density profiles also implied that there was almost no difference in the mean stratification between the mean eastward and westward flows over the EFGB. Moreover, the mean density was used to estimate an average buoyancy frequency (N, the squared buoyancy frequency is defined as: $N^2 = (g/\rho_o)(d\rho/dz)$, where g is the gravitational acceleration, ρ is the density, z is the depth in meters, and ρ_o is the reference density) shown in Figure 6b. The N profiles displayed some variations with depth and among TCP mooring locations, but very limited variability between the mean flow phases. The mean N values were generally less than 0.03 s^{-1} with the depth average of 0.018 s^{-1} and standard error of 0.001 s^{-1}. Equivalent values for the upper 40 m are 0.016 $\pm$ 0.001 s^{-1} and 0.018 $\pm$ 0.002 s^{-1} for the eastward and westward mean flows, respectively. These two 40 m N means were used in further analyses as representative numbers of the ambient stratification.

4. Flow Patterns and Stratification Over the East Flower Garden Bank

Figures 7 and 8 show current observations from three transects (PT4, PT5, and T3) recorded by shipboard ADCPs between 12:15 UTC on 6 June and 2:30 UTC on 7 June 2011. Figure 8 also displays hourly current

Figure 3. Flow at (a and b) M1 and (c and d) M4: east/west (Figures 3a and 3c) and north/south (Figures 3b and 3d) current components (cm s^{-1}); 40 h low passed data; positive values are toward east and north.

data at four depths from all moorings as well as means estimated from those data averaged over the duration of the survey time period. Moreover, Figure 7 shows density along the three transects. During these passes, the mean flow was eastward. The currents were generally directed toward the east above the bank height on both upstream and downstream (lee) EFGB sides (Figures 7 and 8a). Below the crest on the upstream side, the flow decelerated and diverged horizontally around the bank as indicated by current data shown in Figures 8b–8d. The flow was more complex on the downstream side of the bank. The north/south velocity structure for the PT4 and PT5 sections suggested a presence of a vortex on the lee side of the bank (Figures 7b and 7d). They also indicated that this vortex with speeds as high as 20 cm s^{-1} was cyclonic with a horizontal scale of about 4 km and a finite thickness of about 20 m. Current data along PT4 and PT5 transects were taken within 6 h and were the most applicable to be used for computing a vertical component of the relative vorticity ($\zeta = \frac{\partial v}{\partial x} - \frac{\partial u}{\partial y}$, where u and v are horizontal east/west and north/south velocity components, respectively). Figure 9c shows layer-averaged ζ ($H < 40$ m, $40 \text{ m} \leq H \leq 60$ m, and $H > 60$ m, where H is the depth). The vorticity on the upstream side was negligible and generally close to the noise level of the computations. However, a layer of positive vorticity exceeding 10^{-4} s^{-1} was found at depths between 40 and 60 m on the lee side of the EFGB, where ζ was about a factor of two larger than the planetary vorticity, $f = 6.84 \times 10^{-5}$ s^{-1}. The velocity field close to the bank was not well resolved by the shipboard ADCP measurements, and therefore, estimates of negative vorticity found close to the bank on its lee side were not very reliable. Positive temperature (T') and negative potential density (σ_θ') anomalies (Figures 9a and 9b) estimated from observations collected along the PT4 transect were prevalent between 40 and 60 m and indicated deepening of the isothermals and isopycnals on the lee side of the bank. These variations were partially related to lee-side vortex as well as to internal waves and/or mixing. Anomalies of T' and σ_θ' at a given depth along PT4 were computed by subtracting transect-averaged means. Similar temperature and density variations on the lee side were observed along PT5 (data not shown). Typically, submesoscale cyclonic eddies in the ocean are associated with negative temperature anomalies, contrary to the positive temperature variations observed here. Observations along the T3 transect indicated highly variable currents on the lee side suggesting a plausible eddy-like feature below 40 m (Figures 7e, 7f, and 8d). Furthermore, the current observations shown in Figure 7 seem to imply that there was weak flow toward the bank beneath the vortex.

The flow pattern on the upstream side and over the EFGB was also captured by a dye-release survey conducted just after sections shown in Figures 7a–7d were finished. The dye patch was released approximately at a depth of 30 m (roughly between 23.8 and 24.1 kg m^{-3} isopycnals). It was sampled by the ScanFish and
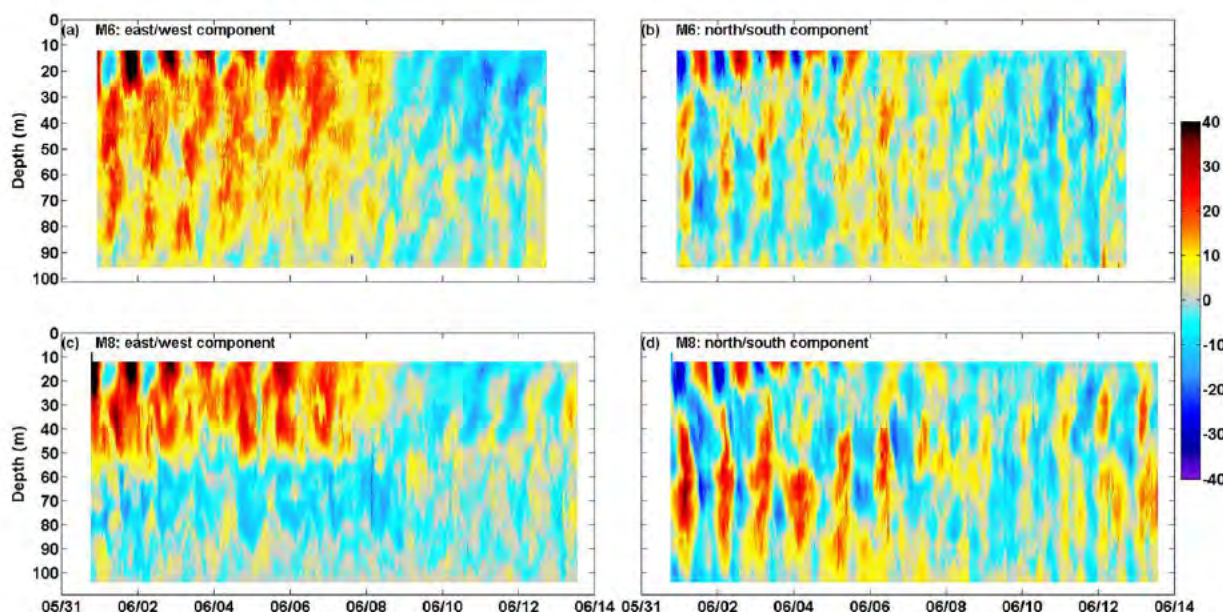
Figure 4. Current velocity components (cm s^{-1}): east/west at (a) M6 and (c) M8 and north/south at (b) M6 and (d) M8; positive values are toward east and north.

the REMUS AUV between 6 and 7 June 2011 (Figure 10a). The dye patch spread vertically between 25 and 45 m depths but it was generally trapped within original density surfaces indicating weak diapycnal mixing. Figure 10b shows a horizontal spreading of the dye with the currents. The currents shown in Figure 10b (black arrows) are averages of those measured between 25 and 45 m by shipboard ADCPs and by moored ADCPs for the time period between 20:00 UTC on 6 June and 14:00 UTC on 7 June 2011. The dye concentration was normalized by dividing by 0.05 ppb, which was the resolution of the fluorometer. The current and the dye concentration structure implied flow divergence on the upstream side with a dye patch being advected by the currents around the southern part of the bank.

Figures 11 and 12 illustrate current and hydrographic fields when the mean flow was westward. Figure 11 displays currents from the shipboard ADCP instruments and density from T8, T9, and T10 transects collected between 13:30 UTC on 11 June and 03:30 UTC on 12 June 2011, while Figure 12 shows velocity vectors along the transects and from the moored ADCPs at four different depths. There were similarities in flow
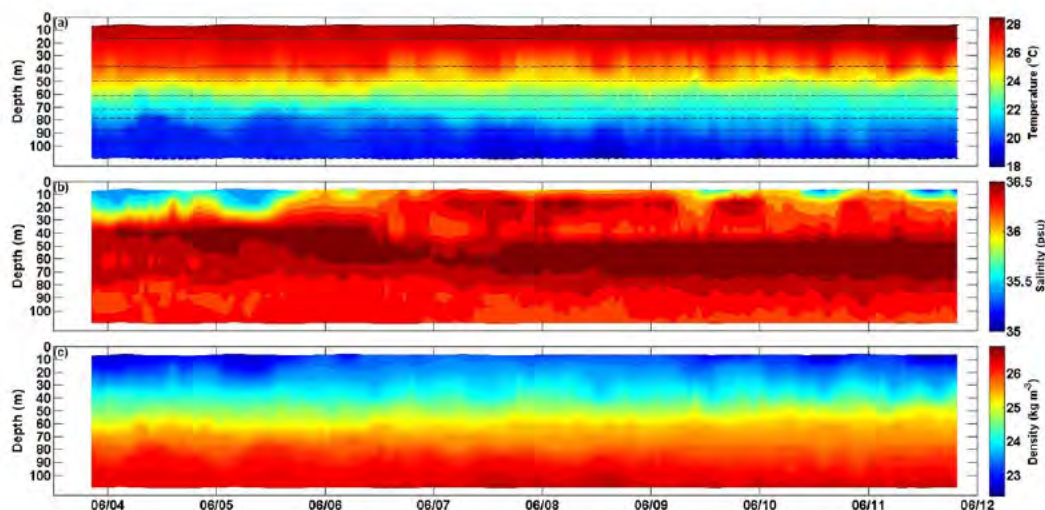

Figure 5. Time series of (a) temperature (°C), (b) salinity (psu), and (c) density (kg m^{-3}) from the S8 mooring; black dashed lines in Figure 5a indicate sensors depths.
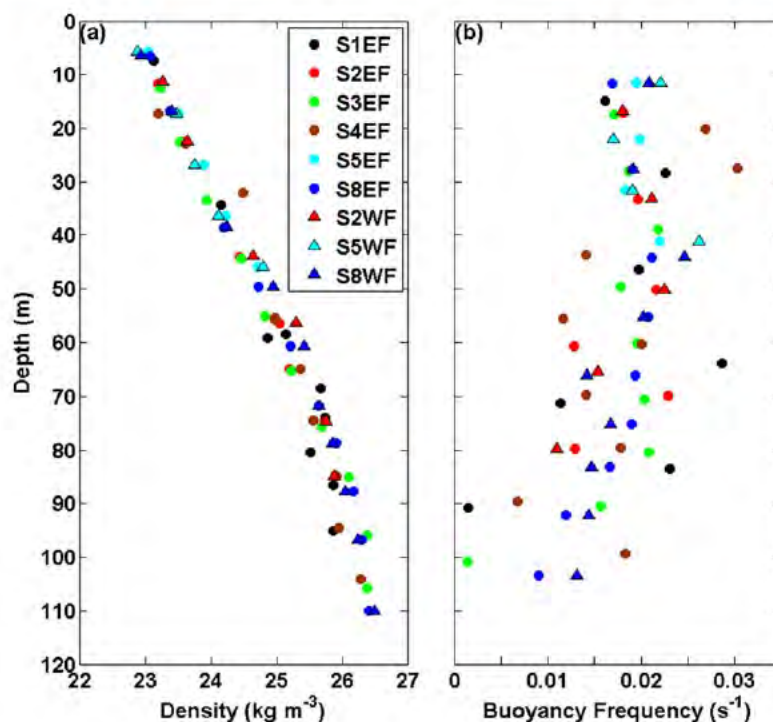
Figure 6. (a) Mean density (kg m^{-3}) and (b) mean buoyancy frequency (s^{-1}) profiles estimated from observations recorded at string moorings (S1 S8) for the mean eastward (EF, circles) and westward (WF, triangles) flow phases.

patterns between both mean flow phases. On the upstream side of the bank, the flow decelerated and diverged near the bank. Similar to the eastward flow, the westward flow tended to generate eddy-like features near mooring M2 on the lee side of the bank (Figures 11c, 11d, 12c, and 12d). The second dye release at a depth of 30 m occurred on 8 June 2011 on the eastern (upstream) side of the EFGB. The vertical spreading of the dye was almost negligible, and the patch was yet again simply advected by the currents over the bank just north of its highest part (Figure 13). The dye experiment showed that there was once more very little vertical mixing, at least along the ScanFish and REMUS tracks and at the depths of the dye release.

Figures 7 and 11 also display examples of potential density (σ_θ) along the transects, while the buoyancy frequency along T4 and T10 is shown in Figure 14. It is obvious from the displayed density and N distributions that waters in the EFGB region were very highly stratified. The upper 40 m of the water column contained a number of well-defined density gradients where the buoyancy frequency was also high (N was often larger than 0.03 s^{-1}). At depths of 3–5 m below the sea surface, there was a first pycnocline (see, for instance, near-surface density in Figure 7e) partially related to a daily temperature cycle, which is quite pronounced in the Gulf of Mexico [*Stommel et al.*, 1969], and partly associated with lower-salinity near the sea surface. The next distinct density gradient displayed in Figure 11 appeared to be associated with salinity variability and was generally at depths between 10 and 15 m depending on a location. The main pycnocline, strongly related to the temperature gradient, was found at depths between 35 and 40 m. Hence, these data suggest that during the experiment there was no mixed layer of significant thickness over the EFGB. An identical assessment was almost true for the bottom boundary layer because the density and N distributions showed that waters were also stratified near the bottom. The thickness of this layer was estimated using potential density. Only waters with $\sigma_\theta > (\sigma_{max} \quad \Delta\sigma)$ were considered within the bottom boundary layer, where σ_{max} is the maximum potential density of each VMP profile and $\Delta\sigma$ 0.01 kg m^{-3}. Estimates of this thickness from density data, which extended nearly to the bottom, showed that the bottom boundary layer was less than 4 m thick for 75% of the VMP profiles. On average, this layer thickness was about 2.3 m (standard deviation 1.5 m and median 1.4 m) and 3.1 m (standard deviation 1.8 m and median 2.5 m) for the eastward and westward mean flow phases, respectively.

5. Turbulence and Mixing

Rough topography on continental shelves is usually characterized by enhanced turbulence and mixing [e.g., *Loder et al.*, 1992; *Moum and Nash*, 2000; *Nash and Moum*, 2001; *Dewey et al.*, 2005]. During the June experiment, flow conditions over the EFGB were weak to moderate and stratification was strong. At the same
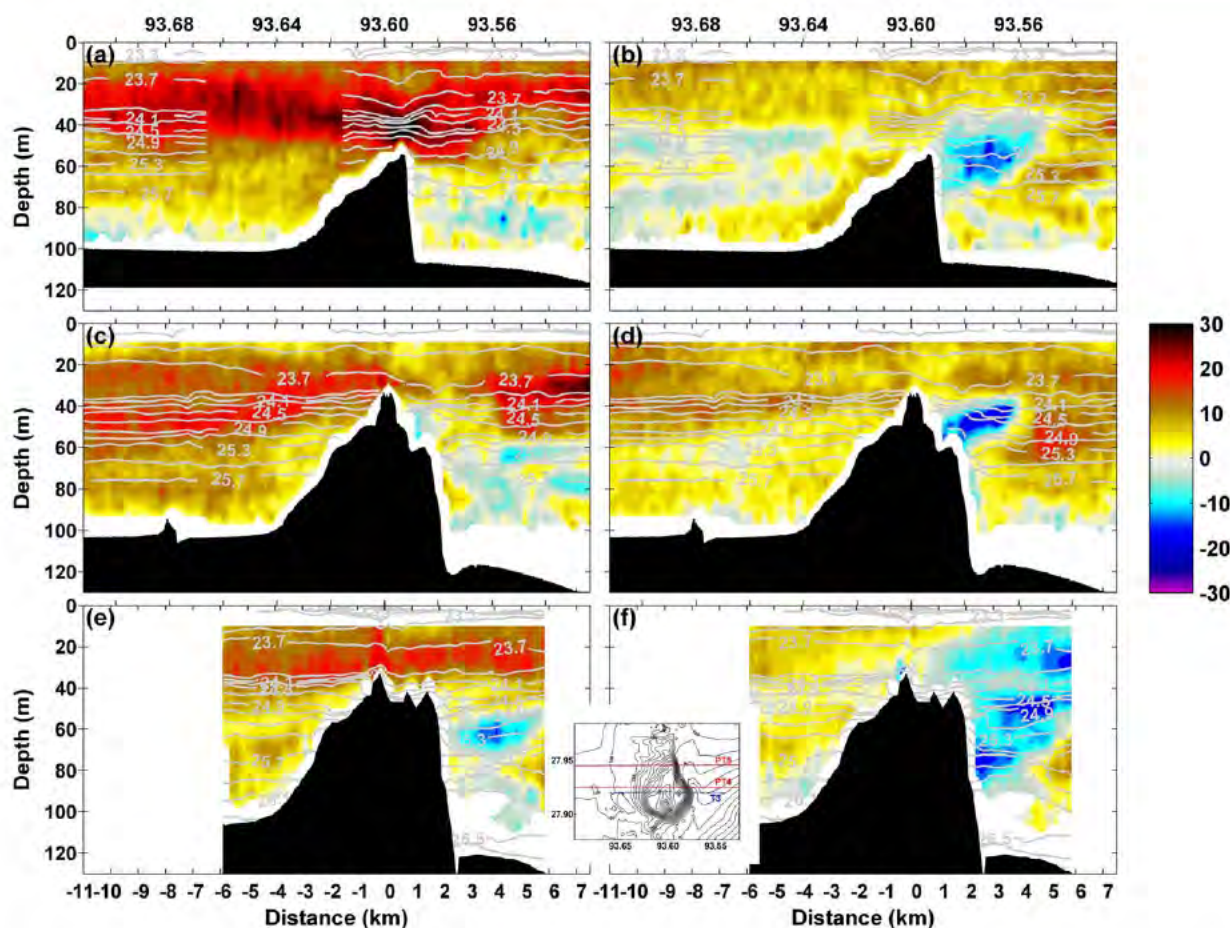
Figure 7. (a, c, and e) East/west and (b, d, and f) north/south current velocities (cm s^{-1}; color bar) from PT5 (Figures 7a and 7b), PT4 (Figures 7c and 7d), and T3 (Figures 7e and 7f) sections taken between 12:15 UTC on 6 June and 2:30 UTC on 7 June 2011 during the mean eastward flow phase; density is also shown (kg m^{-3}; light gray lines plotted every 0.2 kg m^{-3}); top axes in Figures 7a and 7b list longitudes (°; W); the insert shows locations of the transects (measurements along PT4 and PT5 were taken from the R/V Pelican; T3 data were collected from the R/V Manta).

time, however, observed turbulence and mixing over the bank and on its lee side were elevated. Figures 15 and 16 display turbulent kinetic energy dissipation rates (ε) for the eastward and westward mean flows for selected transects, respectively. The dissipation rates were estimated from $\varepsilon \approx \frac{15}{2} v \overline{\left(\frac{\partial u}{\partial z}\right)^2}$ assuming that turbulence was isotropic. This assumption holds when the ratio of ε/vN^2 is larger than 200 [*Gargett et al.*, 1984]. In case of dissipation rates presented in Figures 15 and 16, the ratio was larger than 200 for 14.3% of the ε estimates. *Itsweire et al.* [1993] concluded that an assumption of isotropy may lead to underestimation of ε by factors 2–4 when the ratio is less than 200 and the Richardson number ($Ri \approx N^2 \left(\frac{dU}{dz}\right)^{-2}$, where $\frac{dU}{dz}$ is the horizontal current shear) is larger than 0.37 which was the case during the experiment (more discussion concerning the Richardson numbers estimated from the MORT observations can be found at the end of this section). That means that for 57.6% of the dissipation rate estimates are underestimated. *Itsweire et al.* [1993] also suggested that turbulence produces no significant net buoyancy flux and insignificant mixing if the same ratio is less than 19, which is the case for 28.1% of the estimates here.

The upstream side of the bank was better sampled during the eastward mean flow phase by the microstructure measurements (Figure 15). Except very near the sea surface or the bottom, ε was generally less than 5×10^{-8} W kg^{-1} on the upstream side with depth-averaged means and medians of ε below 10^{-8} W kg^{-1} for each profile. Away from the sea surface and bottom, spatial structures of the dissipations rates also indicate that turbulence was rather intermittent in the water column over the bank and on its downstream side. Some of those turbulent patches on the lee side may have been associated with possible vortices as, for instance, the patches found between depths of 40 and 80 m starting at about 3 km on the lee side of T3 transect where ε was as high as 10^{-6} W kg^{-1} (Figure 15b). High values of ε, which easily reached 10^{-6} W kg^{-1},
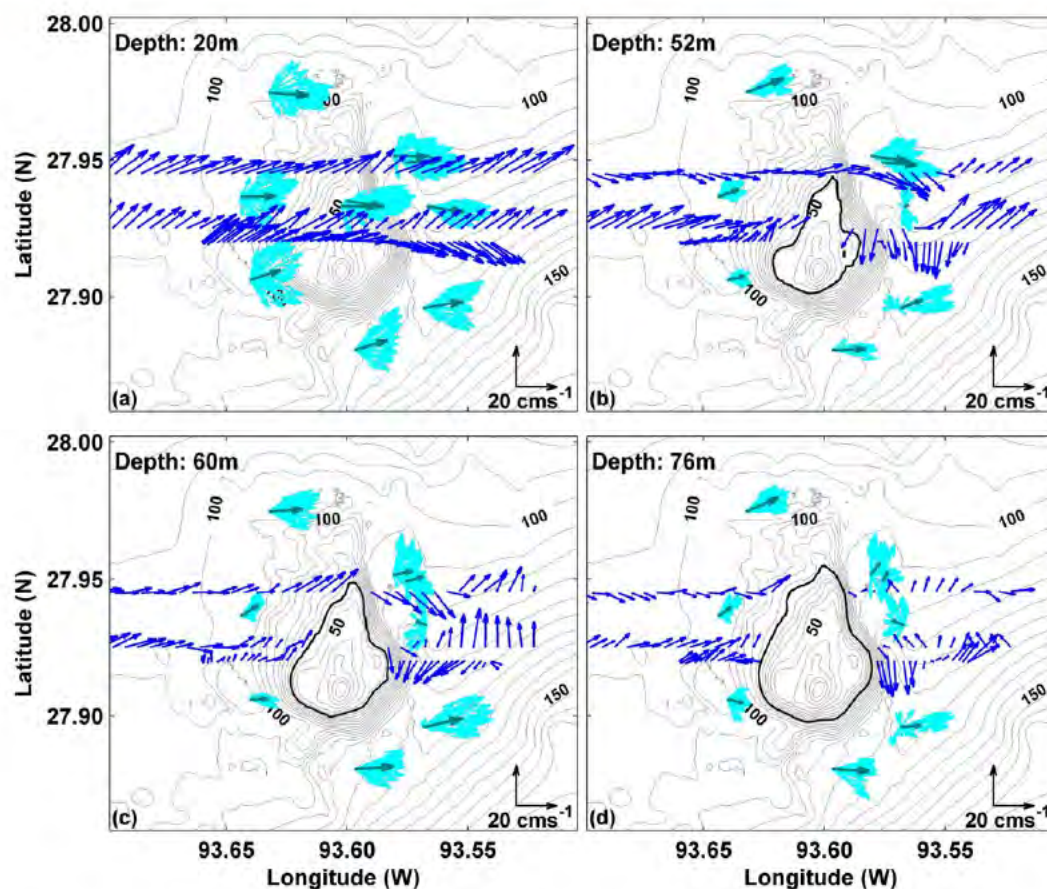
Figure 8. Current velocities (cm s^{-1}) along PT5, PT4, and T3 at (a) 20 m, (b) 52 m, (c) 60 m, and (d) 76 m as measured by shipboard (blue arrows) and moored (cyan arrows) ADCP instruments; also shown are time velocity means (12:15 UTC 6 June to 2:30 UTC 7 June 2011; green arrows) estimated from mooring observations, and depth contours for the chosen depth levels are highlighted by black contour lines.

were also found near the bottom of the EFGB as well as near the sea surface (above 10 m; Figures 15 and 16). Near-surface turbulence seemed to be partially related to the daily temperature cycle since winds were rather weak and surface waves were small and not breaking (surface wave significant heights were less than 0.5 m [*Wijesekera et al.*, 2013]). Additionally, estimates of the Kolmogorov scale (L_O $\varepsilon^{1/2}N^{3/2}$) indicated that length scales of turbulent overturns in the EFGB region were less than 1 m (99% of L_O estimates ≤ 1).

Measured rates of energy dissipation and mixing by turbulence per unit width over the bank and on its downstream side were calculated from $\frac{dE}{dt}$ $\int\int \rho(\varepsilon+J_b)dzdx$, where J_b is the irreversible buoyancy flux that is often approximated by $\Gamma\varepsilon$ (Γ is the mixing efficiency and it is often assumed to be 0.2 [*Osborn*, 1980]). They varied highly among transects. Integrations were done vertically between the first and last depth where energy dissipation rates were available and then horizontally between the foot of the bank on the upstream side to the last available VMP profile on the lee side of the EFGB. For those taken during the mean eastward flow and shown in Figure 15, they were 28.1, 28.5, and 6.5 W m^{-1} for T2, T3, and T4, respectively. Estimates for the T8, T9, and T10 transects, displayed in Figure 16, were correspondingly 13.2, 40.0, and 23.8 W m^{-1}. They also varied temporarily at the same location and for the same mean flow conditions. For instance, for the most northward transect (indicated as T10 in Figure 16), they were 23.8 and 9.7 W m^{-1} as estimated from observations taken about 10 h apart on 12 June 2011.

Following *Osborn* [1980], the eddy diffusivity (K_ρ) was estimated from K_ρ $\Gamma\varepsilon N^{-2}$. It has been shown that the mixing efficiency, Γ, may not be completely constant particularly when stratification is weak [e.g., *Shih et al.*, 2005; *Ivey et al.*, 2008; *Mashayek et al.*, 2013; *Bluteau et al.*, 2013]. For eddy diffusivity estimates discussed here, Γ 0.2 was used as presented in the vast majority of oceanographic mixing literature [see, for
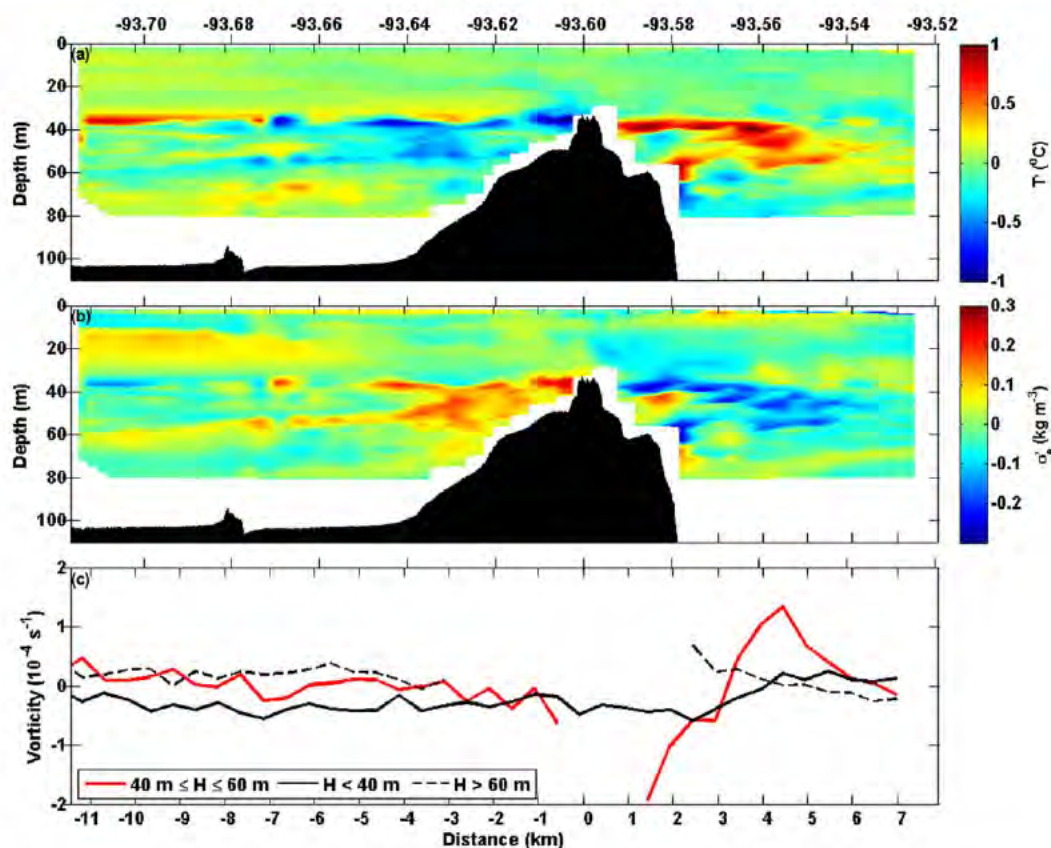
Figure 9. (a) Temperature (T'; °C) and (b) density (σ_θ'; kg m^{-3}) anomalies along PT4, (c) relative vorticity (s^{-1}) estimated from velocity observations from PT4 and PT5; H is the water depth.

example, *Osborn*, 1980; *Oakey*, 1982; *Moum*, 1996; *Nash and Moum*, 2001]. *Gregg et al.* [2012] also provide an extensive discussion and justification for this choice of Γ. Additionally, the eddy diffusivity was estimated only for $N^2 > 10^{-6}$ s^{-2} to avoid a bias toward large values of K_ρ at depths where stratification was very
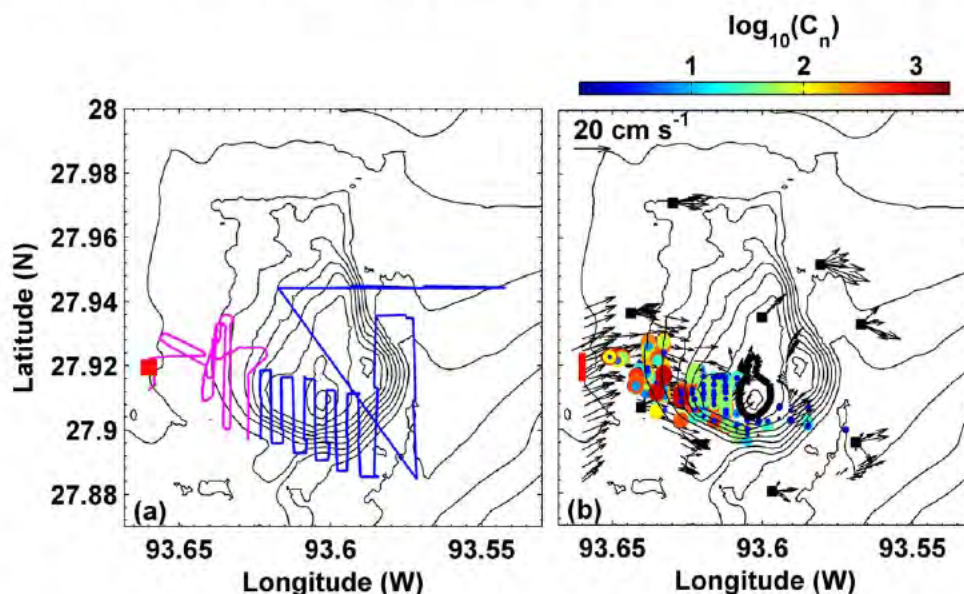
Figure 10. (a) The location (red square) of the dye release on 6 June 2011 and the REMUS (blue) and ScanFish (magenta) survey tracks from 6 to 7 June 2011; (b) normalized dye concentration (color bar) and currents (cm s^{-1}; black arrows).
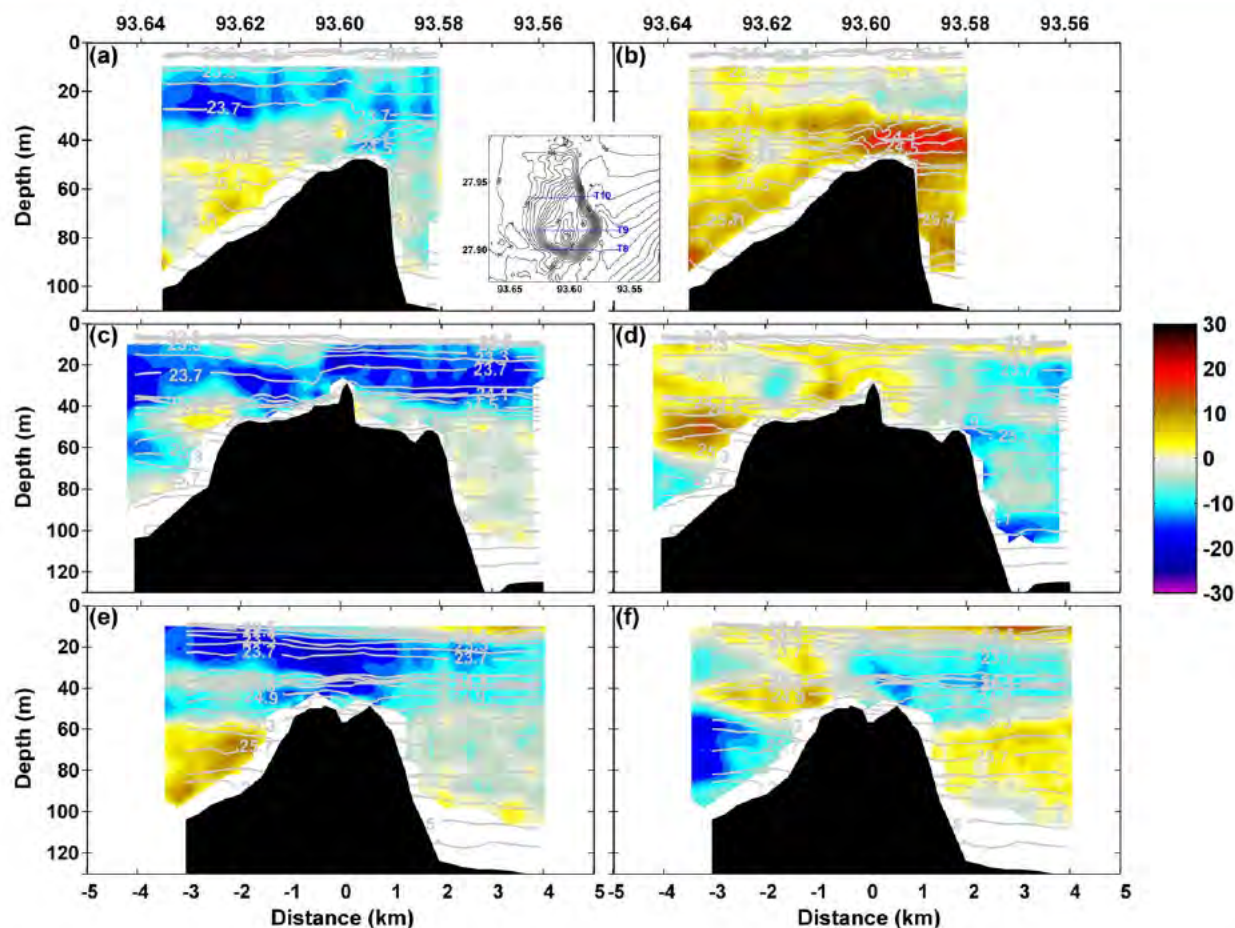
Figure 11. (a, c, and e) East/west and (b, d, and f) north/south current velocities (cm s^{-1}; color bar) from T10 (Figures 11a and 11b), T9 (Figures 11c and 11d), and T8 (Figures 11e and 11f) sections taken between 13:45 UTC on 11 June and 3:30 UTC on 12 June 2011 during the mean westward flow phase; density is also shown (kg m^{-3}; light gray lines plotted every 0.2 kg m^{-3}); top axes in Figures 11a and 11b list longitudes (°; W); the insert shows locations of the transects (measurements along all transects were collected from the R/V Manta).

weak. Estimates of K_ρ spanned from 2.2×10^{-7} to 1.1×10^{-2} m^2 s^{-1} and varied horizontally and vertically. The horizontal variations of the eddy diffusivity along with means and medians for individual profiles are shown in Figure 17 for the T3 and T9 transects. Note that when the approach proposed by *Shih et al.* [2005] is employed and $\varepsilon/\nu N^2 > 100$ (23.1% cases), estimates of the eddy diffusivity are up to an order of magnitude lower than those shown in Figure 17. Upstream of the EFGB, the mixing was rather subdued with K_ρ generally less than 5×10^{-5} m^2 s^{-1}. Such a low values of the eddy diffusivity are representative for mixing over slowly varying topography in the ocean and in the open ocean thermocline. Higher K_ρ ($>10^{-4}$ m^2 s^{-1}) and more vigorous mixing was found over and downstream of the bank. Over the EFGB, estimates of the eddy diffusivity were 10^{-3} m^2 s^{-1} or higher, and elevated mixing was often found near the bottom. On the lee side, similar high K_ρ values were found at depths where the velocity observations implied a presence of vortices. Spatial variability of mixing in the EFGB region was also reflected by results of the dye experiment. For both releases, the dye patches barely spread vertically implying weak vertical mixing as indicated by rather low estimates of the eddy diffusivity, especially on the upstream side of the EFGB. The dye patches were advected horizontally by the currents generally at depths where they were injected.

Despite spatial variations of the eddy diffusivity, turbulent mixing was still more effective and stronger over the EFGB when compared to that over the flat or slowly varying bottom of the continental shelf. One way to compare mixing proficiency is to evaluate total diapycnal buoyancy fluxes over the bank and shelf areas, i.e., $J_b A_b$ and $J_s A_s$ where J_b, J_s are the fluxes and A_b, A_s are the areas of the bank and shelf, respectively. The fluxes are defined as $J_b = K_{\rho b} N_b^2$ and $J_s = K_{\rho s} N_s^2$, where $K_{\rho b}$, $K_{\rho s}$ are eddy diffusivities and N_b^2, N_s^2 are squared buoyancy frequencies for the bank and the shelf, respectively. Following *Lueck and Mudge* [1997], the area
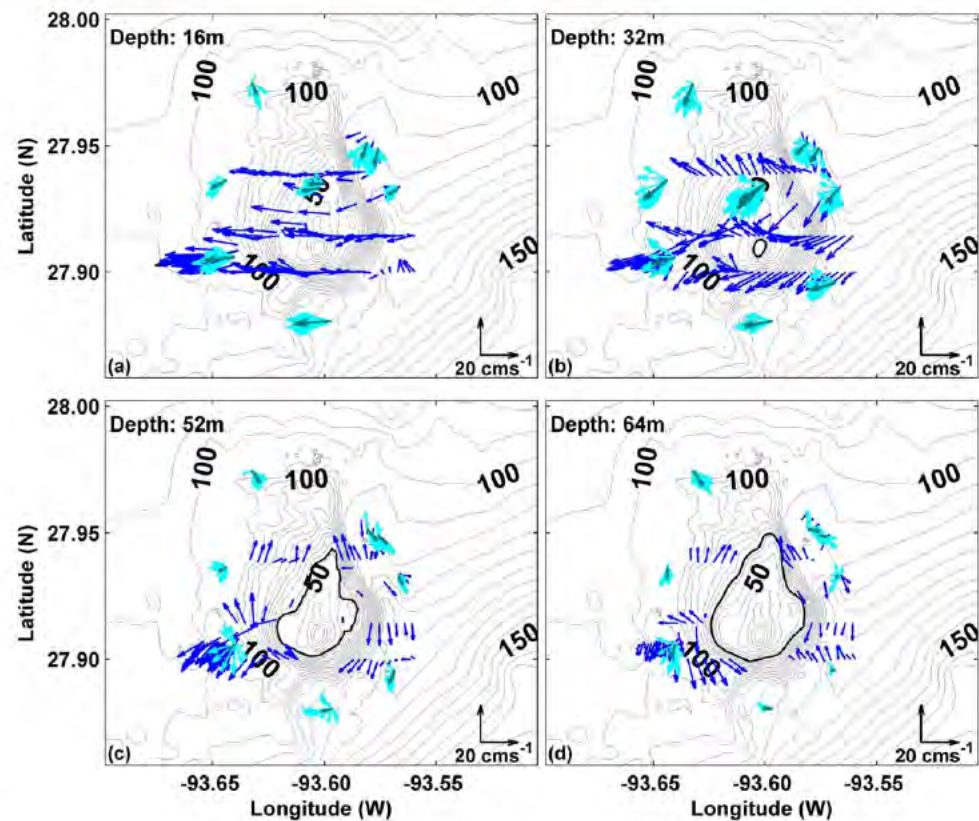
Figure 12. Current velocities (cm s^{-1}) along T8, T9, and T10 at (a) 16 m, (b) 32 m, (c) 52 m, and (d) 64 m as measured by shipboard (blue arrows) and moored (cyan arrows) ADCP instruments; also shown are time velocity means (13:45 UTC 11 June to 3:30 UTC 12 June 2011; green arrows) estimated from mooring observations, and depth contours for the chosen depth levels are highlighted by black contour lines.

of a flat-bottom shelf, which is required to perform as efficient mixing as that over the EFGB, can be estimated by setting J_bA_b J_sA_s. The area of the EFGB within a 100 m isobath is about 40.76 km^2. Taking a typical value of the eddy diffusivity for the shelf, $K_{\rho s}$ 10^5 m^2 s^1, and those estimated for the EFGB,
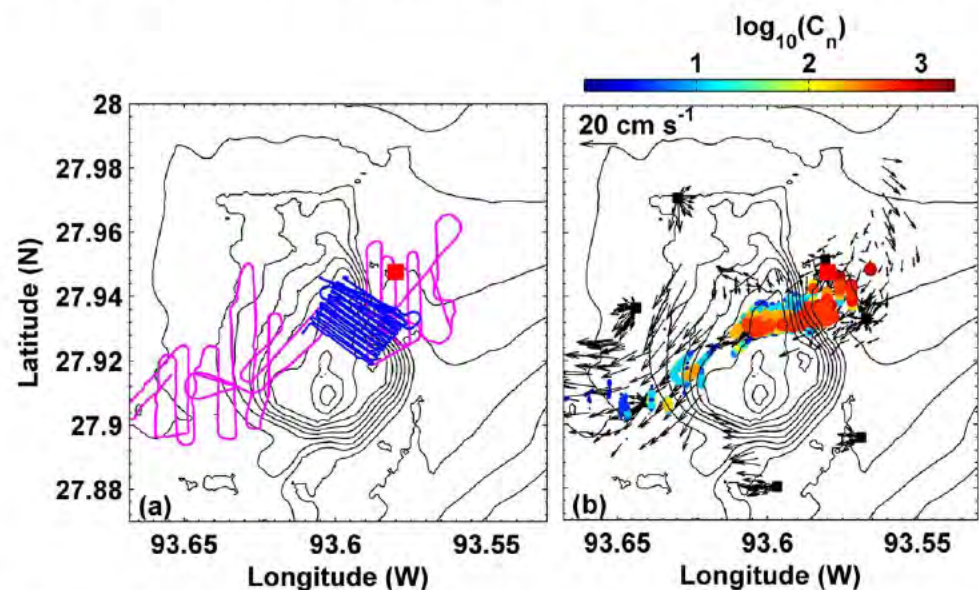

Figure 13. (a) The location (red square) of the dye release on 8 June 2011 and the REMUS (blue) and ScanFish (magenta) survey tracks from 8 to 9 June 2011; (b) normalized dye concentration (color bar) and currents (cm s^{-1}; black arrows).
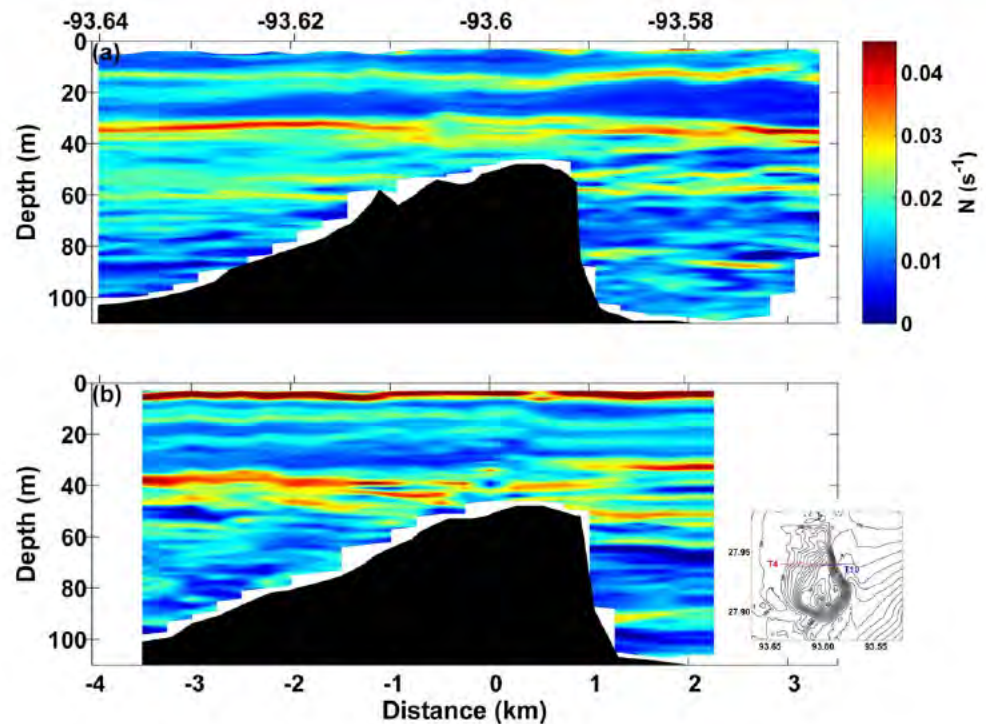
Figure 14. Buoyancy frequency (s^{-1}) along (a) T4 and (b) T10 transects; the insert shows locations of the transects.
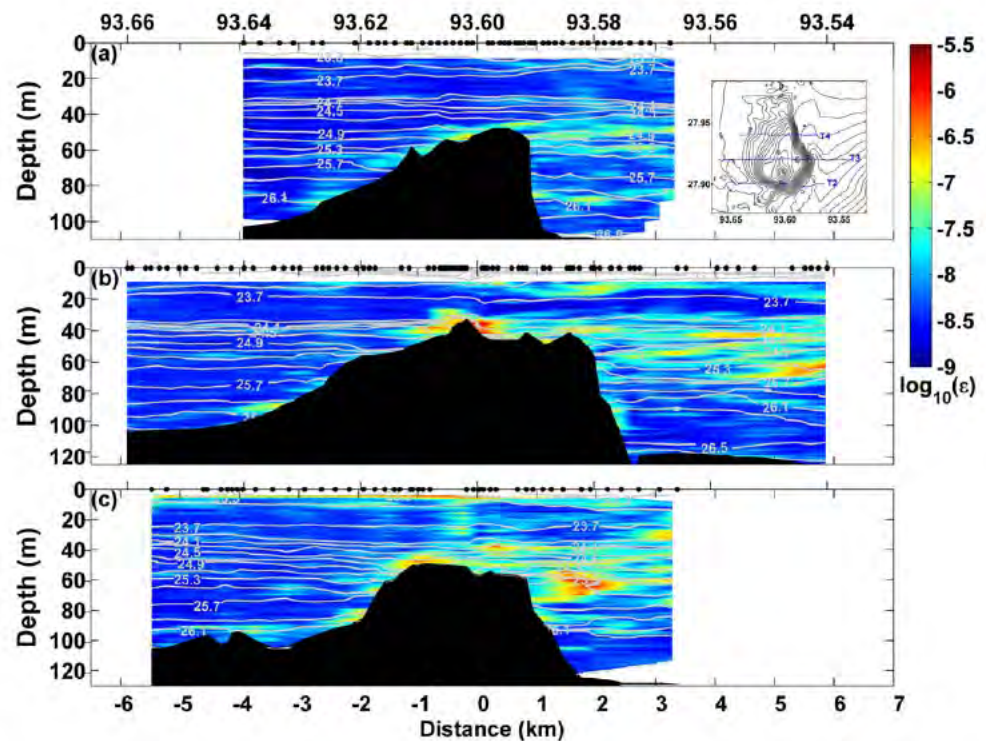

Figure 15. Turbulent kinetic energy (TKE) dissipation rates (ε; W kg^{-1}) along (a) T4, (b) T3, and (c) T2 transects; the top axis in Figure 15a lists longitudes (°; W); the insert shows locations of the transects; microstructure observations were taken between 21:00 UTC on 5 June and 00:30 UTC on 8 June 2011 from the R/V Manta during the mean eastward flow phase; locations of the VMP drops are marked by black dots.
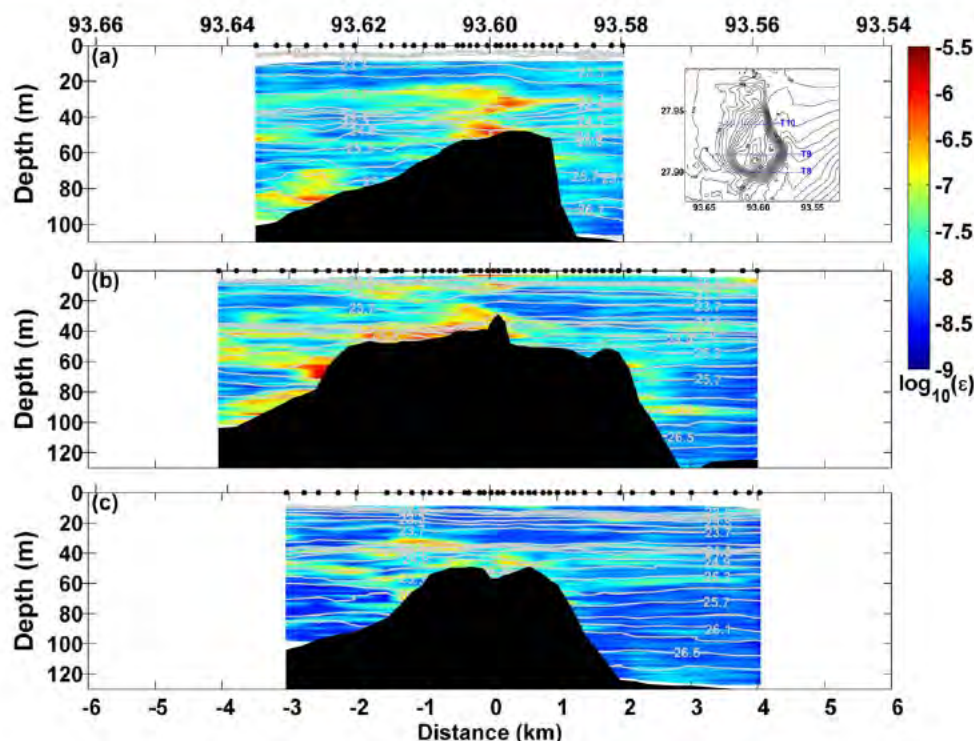
Figure 16. Turbulent kinetic energy (TKE) dissipation rates (ε; W kg^{-1}) along (a) T10, (b) T9, and (c) T8 transects; the top axis in Figures 16a lists longitudes (°; W); the insert shows locations of the transects; microstructure observations were taken between 13:45 UTC on 11 June and 3:30 UTC on 12 June 2011 from the R/V Manta during the mean westward flow phase; locations of the VMP drops are marked by black drops.

$K_{\rho b}$ 10^{-4} 10^{-3} m^2 s^{-1}, and assuming that $N_b^2 \sim N_s^2$, the shelf area has to be from 10 to 100 times larger than that of the bank, i.e., it should be between 407.6 and 4076 km^2.

The velocity and hydrographic observations taken by the shipboard ADCP and the VMP profiler were also used to calculate the Richardson number (estimates not shown) along transects shown in Figures 15 and 16. Values of Ri were rather underestimated due to coarse vertical resolution of the current velocity observations (4 m); thus, higher-resolution current observations are required to obtain a more accurate spatial Ri distribution and to fully understand mixing over the EFGB. Additionally, the Richardson number was estimated only for the squared current shear and N^2 larger than 10^{-6} s^{-2} to avoid a bias toward very small values of Ri at depths where the current shear was low or/and stratification was weak. The distribution of Ri does not indicate that mixing in the EFGB region was mainly related to shear instabilities, i.e., the Richardson number was rarely found to be 0.25 or less. Ri was generally above 1 on the upstream side. The smaller values of the Richardson number at some depths, even as low as 0.25 or less, were mostly found on the downstream side and over the crest of the bank.

6. Discussion

Flows over obstacles are often described in terms of dimensionless parameters. Among those parameters, more common ones are: the Froude number (F_o $\pi U/NH$), a quantity often referred to as the topographic Froude number (F_h U/Nh), the Rossby number (Ro U/fL), the nondimensional obstacle width (l_n Nl/U) and height (h_n h/H) where h is the obstacle height, l is the half of the obstacle width (L), H is the finite upstream depth, U is the upstream flow speed, and f is the Coriolis parameter [see, for example, *Hunt and Snyder*, 1980; *Baines*, 1995, *Vosper et al.*, 1999]. Moreover, the ratio (a_n) of the flow depth (H 100 m) to the obstacle width (L 6000 m) is a good measure whether the flow is hydrostatic. If a_n is much less than one, i.e., for an obstacle with a long horizontal scale, the flow is assumed to be hydrostatic, which is a good approximation for the EFGB for which this ratio is $\sim 10^{-2}$. The rotational effects were also important in this region since Ro was 0.33 (the Ro standard error 0.06; f 6.84 × 10^{-5} s^{-1}).
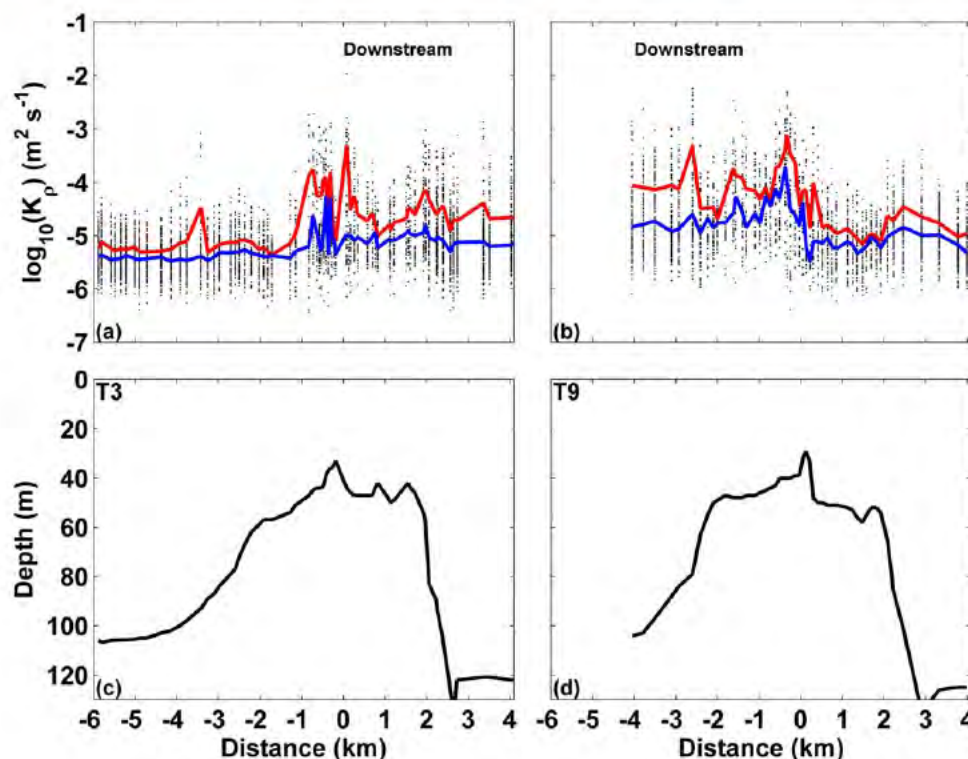
Figure 17. (a and b) Eddy diffusivities ($m^2\,s^{-1}$) and (c and d) bathymetry for T3 (Figures 17a and 17c) and T9 (Figures 17b and 17d) transects; means and medians of eddy diffusivities for each profile are marked by red and blue lines, respectively.

The nondimensional obstacle width, which is larger than 100 for the EFGB, determines if the flow produces dispersive, nonhydrostatic waves ($l_n < 10$) or hydrostatic waves confined mostly to the region near the obstacle ($l_n > 10$). This number indicates that the latter scenario was a possibility in the EFGB region, and the density structure (e.g., Figure 7e) seems to indicate that wave-like features were generated over the bank top. Additionally, the nondimensional height (h_n) of the EFGB varies but is not larger than 0.82 (a h maximum $\sim$ 82 m) and for a major part of the bank, i.e., for 82% of the EFGB area, h_n is below 0.5. h_n is not likely to be important unless it is very close to 1. In such a case, the free surface may interact with an obstacle and generated disturbances are confined vertically. For the EFGB, that may be the case only at its very small southern part where the bank is over 80 m high. Previous research of the flow over a three-dimensional obstacle also has shown that the response, especially on a lee side of the obstacle, strongly depends on its shape and asymmetry [e.g., *Baines*, 1995]. The observations presented here imply that interactions between the free-stream flow and the asymmetric EFGB were very complex during the field experiment.

The Froude number can be used to classify flows over topography. In ocean science, the classically defined Froude number is based on the first-mode internal wave speed (c_o) (e.g., F_o U/c_o $\pi U/NH$, where c_o NH/π). If $F_o > 1$, linear internal waves do not propagate upstream, while if $F_o < 1$ it is possible that the first wave mode (at least) may propagate upstream as a shear front or columnar disturbance mode [e.g., *Wei et al.*, 1975; *Baines*, 1977]. It is also utilized for flow descriptions in the hydraulic sense. *Lawrence* [1993] has distinguished four basic flow regimes: subcritical, crest-controlled, approach-controlled, and supercritical. The flow is referred to as subcritical if F_o is very low ($\ll 1$). Transitional crest-controlled and approach-controlled flows occur in intermediate F_o (~ 1), while supercritical flows are characterized by $F_o > 1$. During the time period (4–12 June 2011) of the extensive sampling over the EFGB, hourly estimates of F_o were always below 0.51. For the eastward mean flow, its average values (averaged over a time used to collect observations along a transect) and their standard errors (in parentheses) were 0.38 ($\pm$0.02), 0.32 ($\pm$0.01), and 0.25 ($\pm$0.01) for T2, T3, and T4, respectively. All F_o values were below 0.20 for the westward mean flow, e.g., the transect means were 0.11 ($\pm$0.01), 0.09 ($\pm$0.01), and 0.17 ($\pm$0.02) for T8, T9, and T10, respectively. H was taken as 100 m and estimated 40 m depth averages of N and U were used in the F_o calculations. These

transect-averaged Froude numbers were much less than 1 indicating that the flow was subcritical during the experiment in the EFGB region.

Estimated mean topographic Froude numbers, which are commonly used in atmospheric research to study airflows over mountainous terrains, were less than 0.25 for all transects regardless of the mean flow phase, and these small numbers clearly imply that the flow was also subcritical and highly nonlinear. It has been shown that highly stratified flows with small F_o and F_h numbers are spatially and temporally variable with nonlinear effects being important [e.g., *Baines*, 1979; *Hunt and Snyder*, 1980; *Smolarkiewicz and Rotunno*, 1989; *Ding et al.*, 2003] when compared, for instance, to weakly stratified flows with Froude numbers larger than 1 [e.g., *Smith*, 1988]. Moreover, these subcritical-highly stratified flows are blocked on the upstream side of the obstacle and tend to move around it [e.g., *Brighton*, 1978; *Baines*, 1979; *Hunt and Snyder*, 1980]. This is the case here, i.e., even though the observations were spatially very coarse they still were able to capture the decelerated and diverged flow on the upstream side of the EFGB (Figures 7, 8, 11, and 12). *Sheppard* [1956] postulated that fluid parcels originated at depth levels above that of $h(1 - F_h)$ would pass over the top. Unfortunately, the observations did not resolve exact depth levels where a separation between fluid parcels going over and those flowing around occurred for the entire EFGB during the experiment; however, applying this approach to T3 and PT4 transects, only fluid at depths above $0.8h$ ($\sim$44 m) would pass over the bank, while fluid at and below that depth would move around the bank (the bank height (h) $\sim$ 70 m). The current velocity observations from these two transects show that the flow was over the bank approximately to 40 m below the sea surface, i.e., just above the depth estimated from Sheppard's criterion, whereas the flow decelerated and began moving along the bank below 40 m.

Previous laboratory and numerical studies [e.g., *Baines*, 1979; *Hunt and Snyder*, 1980; *Smolarkiewicz and Rotunno*, 1989; *Schär and Durran*, 1997; *Vosper et al.*, 1999] have shown that a wake filled with vortices develops on the lee side of an obstacle for subcritical flows. The lee wake is usually characterized by elevated turbulence levels and mixing when compared to those observed on the upstream side of the obstacle. The studies have also shown that vortex shedding occurs generally when F_h falls below 0.4 [*Vosper et al.*, 1999], and that shed vortices are considered to be a means of dissipating flow energy [*Schär and Durran*, 1997]. Our current velocity measurements and estimated relative vorticity indicate that there was a cyclonic vortex on the lee side (the near M4 and M4a moorings; see Figure 1 for their locations) of the EFGB during the mean eastward flow. Results from numerical simulations by *Schär and Durran* [1997] show that all shed cyclonic and anticyclonic vortices are warm-core vortices, which may explain positive temperature anomalies observed in the cyclonic vortex near M4 and M4a. An eddy-like structure emerging from the current observations was less clear for the mean westward flow; however, the data seem to imply that a vortex was generated on the lee side of the bank near M2 (see Figure 1 for the mooring location). Our observations are not sufficient to speculate whether vortices observed during the subcritical flow conditions in the EFGB area were consistent features that were generated by the mean currents, or if they were periodic features forced by tidal/inertial flows, or if they resulted from a combination of both motions. Moreover, the collected microstructure data clearly show that turbulence and mixing, as expected, were enhanced on the downstream side when compared to those on the upstream side of the EFGB for both mean flow phases (Figures 15–17). Enhanced turbulence was patchy and was partly related to vortices.

Furthermore, recent analyses of the pressure distribution by *Wijesekera et al.* [2014] have shown that the highly stratified, nonlinear, hydrostatic flow generated high form drag over the EFGB. The form drag occurs when currents flow over rough topography creating a pressure difference between the upstream and downstream sides of an obstacle, i.e., a force that opposes the flow [e.g., *Moum and Nash*, 2000; *Edwards et al.*, 2004; *Warner et al.*, 2013; *Warner and MacCready*, 2014]. This drag ranged from about 2000–3000 N m^{-1} and shows multiple time scale variability over the EFGB. Similarly, estimated average frictional drag over the bank was also quite high ($\sim$0.006). These findings are in agreement with those reported for other underwater banks [e.g., *Moum and Nash*, 2000].

7. Conclusions and Summary

Beginning on 4 June 2011, a 9 day extensive oceanographic survey was conducted over the East Flower Garden Bank, a coral reef, located in the northwestern Gulf of Mexico about 190 km southeast of Galveston, TX. The EFGB is considered a rough topographic feature. It is about 6 km wide, 10 km long, and is located at the shelf edge in 100 m of water depth with a peak rising to about 18 m below the sea surface. The field experiment involved two research vessels, the R/V Manta and the R/V Pelican. Observations were collected

by shipboard (ADCP), ship-towed (ScanFish), ship-deployed (VMP), autonomous (AUV), and moored (TCP string and ADCP moorings) instrumentation. These data were then used to characterize the flow variability, stratification, turbulence, and mixing over the surveyed bank.

During the experiment, the mean currents over the EFGB switched from eastward to westward on 8 June 2011. The measured flow was a combination of the subtidal, inertial, tidal, and higher-frequency motions with a maximum speed of about 50 cm s^{-1}. The waters were highly stratified throughout the entire water column with the depth mean buoyancy frequency of 0.016 and 0.018 s^{-1} for the eastward and westward mean flow phases, respectively. As a result, the mixed surface and bottom boundary layers were generally less than 4 m thick. Consequently, the flow conditions over the EFGB were classified as subcritical when transects were sampled since all estimated Froude numbers (F_o) were less than 0.4. Based on computed nondimensional parameters (a_n, l_n, F_h, h_n, and Ro), flow dynamics over the bank were also hydrostatic, non-linear, and rotational effects were important.

Observations clearly showed that flow structure and mixing were highly dependent on the direction and strength of the currents in the EFGB region; thus, they varied spatially and temporarily. As past observational, laboratory, and numerical efforts [e.g., *Baines*, 1979; *Hunt and Snyder*, 1980; *Smolarkiewicz and Rotunno*, 1989; *Vosper*, 2000; *Nash and Moum*, 2001; *Skyllingstad and Wijesekera*, 2004; *Dewey et al.*, 2005] have indicated, responses resulting from interactions between the free-stream flow and the bank were significantly different on the upstream and lee sides of the EFGB. For highly stratified, subcritical flows over an obstacle, blocking and diverging of the flow is expected on its upstream side, and these flow features were observed on the upstream side of the EFGB for both mean eastward and westward current phases. On the downstream side of the bank, a wake developed as identified by past studies of flows with low Froude numbers. The current observations and estimated relative vorticity also implied that eddy-like features were present on the lee side of the bank. Furthermore, turbulence was amplified over the EFGB top and on its lee side. Estimated TKE dissipation rates from small-scale velocity shear observations were as high as 10^{-6} W kg^{-1} resulting in measured rates of energy dissipation and mixing by turbulence per unit width over the bank as high as 40 W m^{-1}. Even for such weak flow conditions, mixing on the downstream side was also enhanced by a few orders of magnitude above the typical shelf value of 10^{-5} m^2 s^{-1}, and the eddy diffusivity there was as high as 10^{-3} m^2 s^{-1}. On the upstream side, estimated values of K_ρ were close to that for the continental shelf with gradually varying bathymetry and were generally less than 0.5×10^{-4} m^2 s^{-1}.

Significantly stronger flows over the EFGB were recorded by the year-long moorings (M1–M5) [*Teague et al.*, 2013]. Turbulence and mixing are expected to be more elevated during the more extreme currents commonly observed in the EFGB region than turbulence and mixing observed during our 9 day intense oceanographic survey. Hence, the coral reefs can be considered as "hot spots" for mixing on the shelf in the northwestern Gulf of Mexico.

References

Baines, P. G. (1977), Upstream influence and Long's model in stratified flows, *J. Fluid Mech.*, 82, 147 159.

Baines, P. G. (1979), Observations of stratified flow past three dimensional barriers, *J. Geophys. Res.*, 84, 7834 7838.

Baines, P. G. (1995), *Topographic Effects in Stratified Flows*, Cambridge Univ. Press, Cambridge, U. K.

Bluteau, C. E., N. L. Jones, and G. N. Ivey (2013), Turbulent mixing efficiency at an energetic ocean site, *J. Geophys. Res. Oceans*, 118, 4662 4672, doi:10.1002/jgrc.20292.

Brighton, P. W. M. (1978), Strongly stratified flow past three dimensional obstacles, *Q. J. R. Meteorol. Soc.*, 104, 289 307.

Chen, C., R. O. Reid, and W. D. Nowlin (1996), Near inertial oscillations over the Texas Louisiana shelf, *J. Geophys. Res.*, 101, 3509 3524.

Dalziel, S. B., M. D. Patterson, C. P. Caulfield, and S. Le Brun (2011), The structure of low Froude number lee waves over an isolated obstacle, *J. Fluid Mech.*, 689, 3 31.

Dewey, R., D. Richmond, and C. Garrett (2005), Stratified tidal flow over a bump, *J. Phys. Oceanogr.*, 35, 1911 1927.

Dewey, R. K., and W. R. Crawford (1988), Bottom stress estimates from vertical dissipation rate profiles on the continental shelf, *J. Phys. Oceanogr.*, 18, 1167 1177.

DiMarco, S. F., and R. O. Reid (1998), Characterization of the principle tidal current constituents on the Texas Louisiana shelf, *J. Geophys. Res.*, 103, 3093 3109.

Ding, L., R. J. Calhoun, and R. L. Street (2003), Numerical simulation of strongly stratified flow over a three dimensional hill, *Boundary Layer Meteorol.*, 107, 81 114.

Edwards, K. A., P. MacCready, J. N. Moum, G. Pawlak, J. Klymak, and A. Perlin (2004), Form drag and mixing due to tidal flow past a sharp point, *J. Phys. Oceanogr.*, 34, 1297 1312.

Farmer, D. M., and L. Armi (1999), The generation and trapping of solitary waves over topography, *Science*, 283, 188 190.

Firing, E., J. Ranada, and P. Caldwell (1995), *Processing ADCP Data With the CODAS Software System Version 3.1, User's Manual*. [Available at http://currents.soest.hawaii.edu/docs/doc/codas doc/.]

Gargett, A. E., T. R. Osborn, and P. W. Nasmyth (1984), Local isotropy and decay of turbulence in a stratified fluid, *J. Fluid Mech.*, 144, 231 280.

Gregg, M. C. (1987), Diapycnal mixing in the thermocline: A review, *J. Geophys. Res., 92*, 5249 5286.

Gregg, M. C., M. H. Alford, H. Kontoyiannis, V. Zervakis, and D. Winkel (2012), Mixing over the steep side of the Cycladic Plateau in the Aegean Sea, *J. Mar. Syst., 89*, 30 47, doi:10.1016/j.jmarsys.2011.07.009.

Gutierrez de Velasco, G., and C. D. Winant (1996), Seasonal patterns of wind stress and wind stress curl over the Gulf of Mexico, *J. Geophys. Res., 101*, 18,127 18,140.

Hogg, A. M., G. N. Ivey, and K. B. Winters (2001), Hydraulics and mixing in controlled exchange, flows, *J. Geophys. Res., 108*, 959 972.

Hunt, J. C. R., and W. H. Snyder (1980), Experiments on stably and neutrally stratified flow over a model three dimensional hill, *J. Fluid Mech., 96*, 671 704.

Itsweire, E. C., J. R. Koseff, D. A. Briggs, and J. H. Ferziger (1993), Turbulence in stratified shear flows: Implication for interpreting shear induced mixing in the ocean, *J. Phys. Oceanogr., 23*, 1508 1522.

Ivey, G. N., K. B. Winters, and J. R. Koseff (2008), Density stratification, turbulence, but how much mixing?, *Annu. Rev. Fluid Mech., 40*, 169 184.

Kunze, E., and J. M. Toole (1997), Tidally driven vorticity, diurnal shear, and turbulence atop Fieberling Seamount, *J. Phys. Oceanogr., 27*, 2663 2693.

Lawrence, G. A. (1993), The hydraulics of steady two layer flow over a fixed obstacle, *J. Fluid Mech., 254*, 605 633.

Ledwell, J. R., A. J. Watson, and C. S. Law (1993), Evidence for slow mixing across the pycnocline from an open ocean tracer release experi ment, *Nature, 364*, 701 703.

Loder, J. W., D. Brickman, and E. P. W. Horne (1992), Detailed structure of currents and hydrography on the northern side of Gorges Bank, *J. Geophys. Res., 97*, 14,331 14,351.

Lueck, R. G., and T. D. Mudge (1997), Topographically induced mixing around a shallow seamount, *Science, 276*, 1831 1833.

Mashayek, A., C. P. Caulfield, and W. R. Peltier (2013), Time dependent, nono monotonic mixing in stratified turbulent shear flows: Implica tions for oceanographic estimates of buoyancy flux, *J. Fluid Mech., 736*, 570 593.

McCabe, R., P. MacCready, and G. Pawlak (2006), Form drag due to flow separation at a headland, *J. Phys. Oceanogr., 36*, 2136 2152.

Moline, M. A., S. M. Blackwell, C. von Alt, B. Allen, T. Austin, J. Case, N. Forrester, R. Goldsborough, M. Purcell, and R. Stokey (2005), Remote environmental monitoring units: An autonomous vehicle characterizing coastal environments, *J. Atmos. Oceanic Technol., 22*, 1797 1808.

Moum, J. N. (1996), Efficiency of nixing in the main thermocline, *J. Geophys. Res., 101*, 12,057 12,069.

Moum, J. N., and J. D. Nash (2000), Topographically induced drag and mixing at a small bank on the continental shelf, *J. Phys. Oceanogr., 30*, 2049 2054.

Moum, J. N., and J. D. Nash (2008), Seafloor pressure measurements of nonlinear internal waves, *J. Phys. Oceanogr., 38*, 481 491.

Nash, J. D., and J. N. Moum (2001), Internal hydraulic flows on the continental shelf: High drag states over a small bank, *J. Geophys. Res., 106*, 4593 4611.

Oakey, N. S. (1982), Determination of the rate of dissipation of turbulent energy from simultaneous temperature and velocity shear micro structure measurements, *J. Phys. Oceanogr., 12*, 256 271.

Osborn, T. R. (1980), Estimates of the local rate of vertical diffusion from dissipation measurements, *J. Phys. Oceanogr., 10*, 83 89.

Polzin, K. L., J. M. Toole, J. R. Ledwell, and R. W. Schmitt (1997), Spatial variability of turbulent mixing in the Abyssal Ocean, *Science, 279*, 93 96.

Rudnick, D. L., et al. (2003), From tides to mixing along the Hawaiian Ridge, *Science, 301*, 355 357.

Schär, C., and D. R. Durran (1997), Vortex formation and vortex shedding in continuously stratified flows past isolated topography, *J. Atmos. Sci., 54*, 534 554.

Sheppard, P. A. (1956), Airflow over mountains, *Q. J. R. Meteorol. Soc., 75*, 528 529.

Shih, L. H., J. R. Koseff, G. N. Ivey, and J. H. Ferziger (2005), Parameterization of turbulent fluxes and scales using homogeneous sheared sta bly stratified turbulence simulations, *J. Fluid Mech., 525*, 193 214.

Skyllingstad, E. D., and H. W. Wijesekera (2004), Large eddy simulation of flow over two dimensional obstacles: High drag states and mixing, *J. Phys. Oceanogr., 34*, 94 112.

Smith, R. B. (1988), Linear theory of stratified flow past an isolated mountain in isosteric coordinates, *J. Atmos. Sci., 45*, 3889 3896.

Smith, R. B., and S. Grønås (1993), Stagnation points and bifurcation in 3 D mountain flow, *Tellus, Ser. A, 45*, 28 43.

Smolarkiewicz, P. K., and R. Rotunno (1989), Low Froude number flow past three dimensional obstacles. Part I: Baroclinically generated Lee vortices, *J. Atmos. Sci., 46*, 1154 1164.

Stommel, H., K. Saunders, W. Simmons, and J. Cooper (1969), Observations of the diurnal thermocline, *Deep Sea Res. Oceanogr. Abstr., 16*, supplement, 269 284.

Teague, W. J., H. W. Wijesekera, E. Jarosz, D. B. Fribance, A. Lugo Fernández, and Z. R. Hallock (2013), Current and hydrographic conditions at the East Flower Garden Bank in 2011, *Cont. Shelf Res., 63*, 43 58.

Teague, W. J., H. W. Wijesekera, E. Jarosz, A. Lugo Fernández, and Z. R. Hallock (2014), Wavelet analysis of near inertial currents at the East Flower Garden Bank, *Cont. Shelf Res., 88*, 47 60.

Vosper, S. B. (2000), Three dimensional numerical simulations of strongly stratified flow past conical orography, *J. Atmos. Sci., 57*, 3716 3739.

Vosper, S. B., I. P. Castro, W. H. Snyder, and S. D. Mobbs (1999), Experimental studies of strongly stratified flow past three dimensional orog raphy, *J. Fluid Mech., 390*, 223 249.

Warner, S. J., and P. MacCready (2014), The dynamics of pressure and form drag on a sloping headland: Internal waves versus eddies, *J. Geophys. Res. Oceans, 119*, 1554 1571, doi.10.1002/2013JC009757.

Warner, S. J., P. MacCready, J. N. Moum, and J. D. Nash (2013), Measurements of tidal form drag using seafloor pressure sensors, *J. Phys. Oceanogr., 43*, 1150 1172.

Wei, S. N., T. W. Kao, and H. P. Pao (1975), Experimental study of upstream influence in the two dimensional flow of a stratified fluid over an obstacle, *Geophys. Fluid Dyn., 6*, 315 336.

Wesson, J. C., and M. C. Gregg (1994), Mixing at Camarinal sill in the Strait of Gibraltar, *J. Geophys. Res., 99*, 9847 9878, doi:10.1029/94JC00256.

Wijesekera, H. W., D. W. Wang, W. J. Teague, E. Jarosz, W. E. Rogers, D. B. Fribance, and J. N. Moum (2013), Surafce wave effects on high frequency currents over a shelf edge bank, *J. Phys. Oceanogr., 43*, 1627 1647.

Wijesekera, H. W., E. Jarosz, W. J. Teague, D. W. Wang, D. B. Fribance, J. N. Moum, and S. J. Warner (2014), Measurements of form and fric tional drags over a rough topographic bank, *J. Phys. Oceanogr., 44*, 2409 2432.

Wolk, F., H. Yamazaki, L. Seuront, and R. G. Lueck (2002), A new free fall profiler for measuring biophysical microstructure, *J. Atmos. Oceanic Technol., 19*, 780 793.